Electronic Supplementary Material (ESI) for Physical Chemistry Chemical Physics.

Electronic Supporting File

Quantitative evaluation of the electronic features involving the "*Nucleophilic-Electrophilic*" Character in the Chalcogen Sulfur

Koushik Mandal, Avantika Hasija, Rahul Shukla*, Venkatesha R. Hathwar* and Deepak Chopra*

List of Contents

S1. Cambridge Structural Database (CSD) search.

We analysed the Conquest module in the Cambridge Structural Database (CSD)[1] (v 5.43) for S···π and S···X interactions (X= Br, N, F, O, S) present in (1A), (1B), (1C), (2A) and (2B). **Figure S1** shows the scheme used for CSD searches. The following search parameters were imposed: Only structures whose 3D coordinates are determined and are error free were involved in the search query. In addition to this, disordered structures, polymers, ionic and powder structures were also excluded from the search.

To ensure that we only have high-quality structures, the R-factor, which represents the agreement between the obtained crystallographic model and the experimental diffraction data was kept at ≤0.05 for the current search. Furthermore, distance and angularity criteria were restricted for all the systems as follows: S···π (aromatic)/ S···X (X= Br, N, F, O, S) contacts with distance 3.50-4.05 Å/3.25-4.05Å were involved in the structures, and θ1 and θ2 both were restricted in the range of 80° - 170° for all sulfur-centered interactions. CSD search showed 1923 hits from Query 1, only 12 hits from Query 3 for S···π, and 3274 hits from Query 2 and only 143 hits from Query 4 for S···X interactions, where X = Br, N, F, O, S (**Table S1**).

Table S1. CSD scheme showing number of hits for sulfur centered interactions

	CSD Scheme	Criteria	Total number of Hits
Query 1	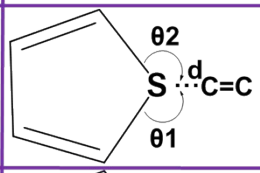	θ1 = θ2 = 80 - 170° d = 3.50 – 4.00 Å	1923
Query 2	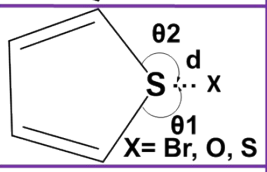	θ1 = θ2 = 80 - 170° d = 3.30 – 3.70 Å	3274
Query 3	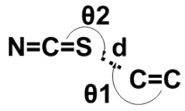	θ1 = θ2 = 80 - 170° d = 3.50 – 4.05 Å	12
Query 4	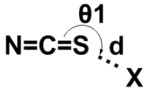	θ1 = 80 - 170° d = 3.25– 4.05 Å	143

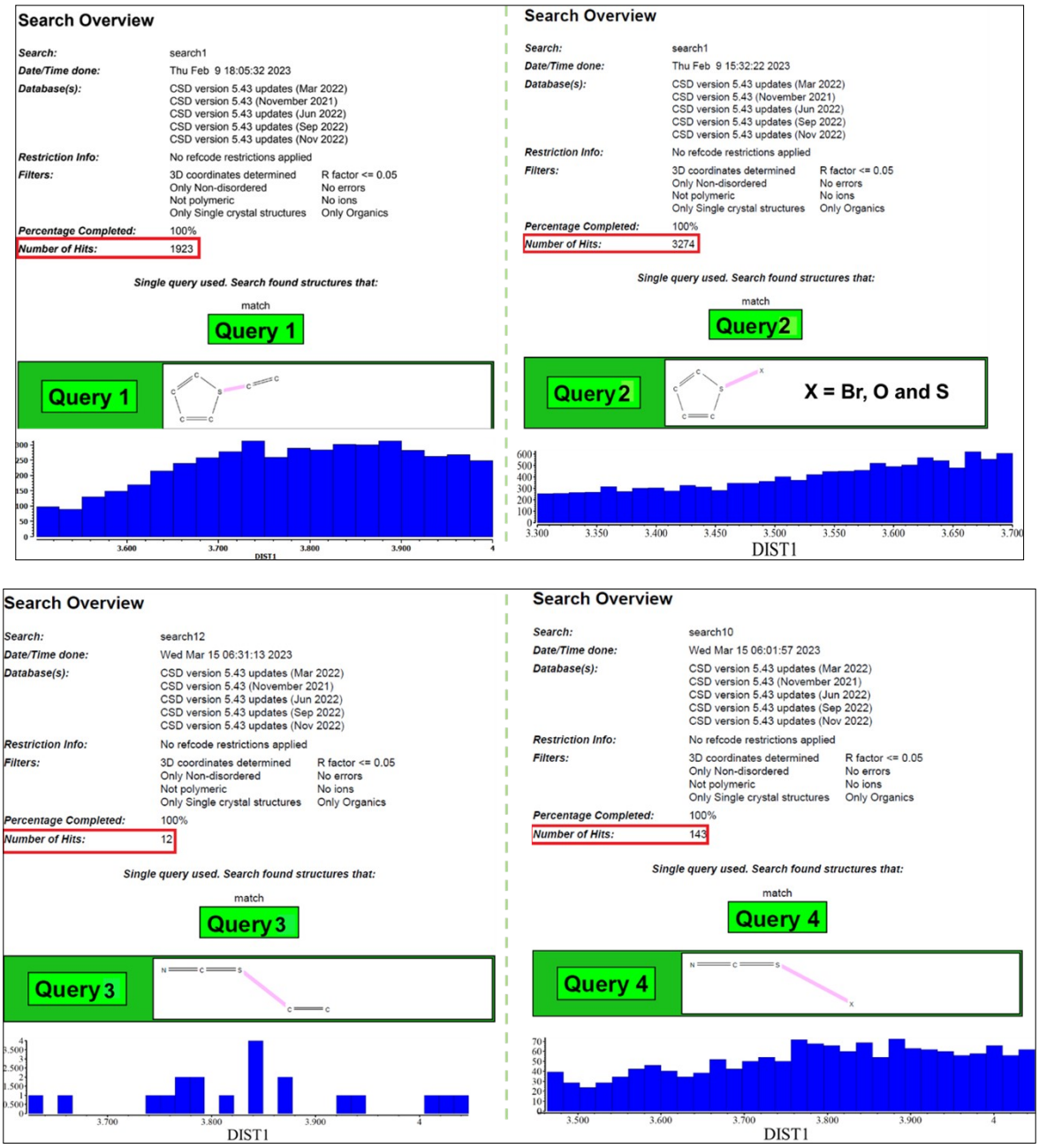

Figure S1. CSD search performed for S···π and S···X interactions (X= F, Br, N, O, S)

S2. ***In situ*** **cryocrystallization, data collection and refinement details for (1A), (1B), (1C), (2A) and (2B).**

The experiments of crystallizing liquids under non-ambient conditions are performed using an optical heating and crystallization device (OHCD) (**Reference 17** in main manuscript). The liquid sample (1A), (1B), (2A) and (2B) was filled in a Lindemann glass capillary (0.3 mm diameter) and sealed from both sides. The capillary was mounted for crystallization under liquid nitrogen flow. After solidification of the sample, via gradual lowering of the temperature, a zone was chosen, which was melted using a CO_2 laser. To start with, these solidified domains

are polycrystalline in nature. In order to obtain single crystals of the sample inside the capillary, an optimization of the rate of flow of liquid nitrogen and the power of the laser through OHCD was performed. The quality of crystals obtained (**Figure S2**) is checked via recording still images of the diffraction event (**Figure S3**). The temperature for obtaining crystals via *in situ* cryocrystallization and the corresponding lattice energies are mentioned in **Table S2.** Compound (**1C**), is a solid at room temperature and pressure, and hence suitable single crystals have been grown from methanol at room temperature via the method of slow evaporation. This resulted in plate-like morphology for the obtained crystals. The SCXRD data for the crystals grown (via *in situ* and solvent evaporation) were collected on Bruker APEX II [2] (3-circle) CCD single crystal diffractometer equipped with Mo Kα monochromatic radiation (λ = 0.71073 Å) at 100 K with only ω-scans (scan width of 0.5°). Data collection, unit cell measurements, integration, scaling, and absorption correction (multi-scan using SADABS) [3] were performed using Bruker APEX II software. The crystal structures were refined with full-matrix least-squares method in SHELXL-2018 [4] present in the program suite Olex2[5]. All non-hydrogen atoms were refined through anisotropic displacement parameters and all the aromatic protons were fixed at idealized positions. All crystallographic data and refinement parameters are mentioned in **Table S3** and **S4** for spherical and aspherical atom refinement respectively. The packing diagrams of all crystal structures were obtained using Mercury 2020.1[6] and geometrical calculations have been performed using PARST[7] and PLATON.[8] **Table S5** lists the relevant interactions observed in the crystal structures of all the molecules in this study.

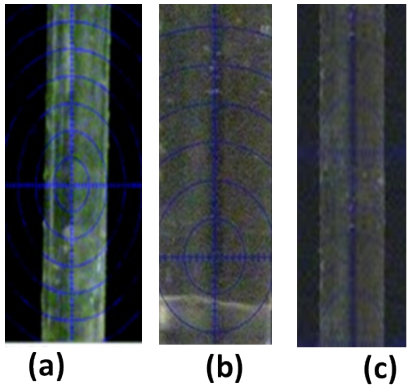

Figure S2. (a) Crystallization inside the Lindemann capillary for (a) (1A) (b) (1B) and (c) (2A).

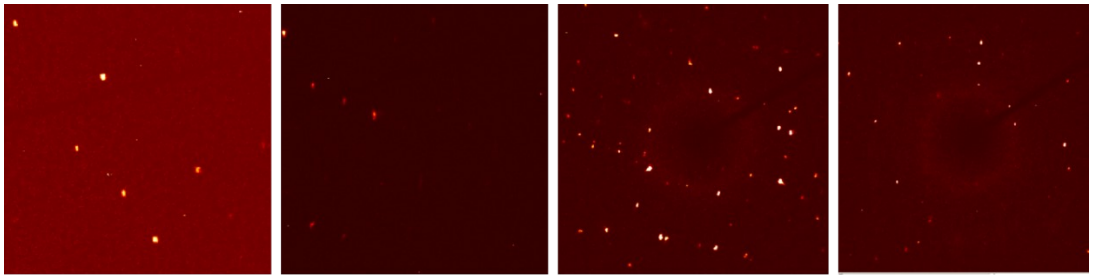

Figure S3. Still image obtained during the diffraction experiments via *in situ* cryocrystallization of (a) (1A) (b) (1B) (c) (2A) and (d) (2B).

Table S2. Temperature for *in situ* cryocrystallization and Lattice Energy (kJ/mol) for thiophenes and phenyl isothiocyanate derivatives.

Molecule	Temperature for *in situ* cryocrystallization (°C)	Lattice energy (kJ/mol)
(1A)	-59	-62.8
(1B)	-78	-67.4
(1C)	25-30(RT)	-80.2
(2A)	-19	-64.3
(2B)	-26	-80.6

Table S3. Crystallographic data and refinement parameters (Spherical atom refinement).

Data	(1A)	(1B)	(1C)	(2A)	(2B)
CCDC	**2210195**	**2210193**	**2210196**	**2210192**	**2210194**
Formula	$C_5H_4O_1S_1$	$C_5H_4O_1S_1$	$C_5H_3Br_1O_1S_1$	$C_7H_5N_1S_1$	$C_8F_3N_1S_1H_4$
Temperature/K	100(2)	100(2)	100(2)	140(1)	140(2)
Solvent/Condition	OHCD (214K)	OHCD (195K)	MeOH (RT)	OHCD (254K)	OHCD (247K)
Crystal system	Orthorhombic	Monoclinic	Monoclinic	Monoclinic	Monoclinic
Space group	$P2_12_12_1$	$P2_1/n$	$P2_1/c$	$P2_1/c$	$P2_1/c$
***a* (Å)**	5.52550(10)	7.2300(4)	4.1013(2)	8.8648(6)	13.2687(4)
***b* (Å)**	5.90890(10)	7.9881(4)	8.5014(3)	4.5145(4)	7.8122(2)
***c* (Å)**	16.0342(4)	8.7762(5)	17.1726(6)	16.9480(16)	8.0302(2)
***α* (°)**	90	90	90	90	90
***β* (°)**	90	91.799(3)	90.856(2)	97.830(8)	91.369(2)
***γ* (°)**	90	90	90	90	90
V(Å^3)	523.511(18)	506.61(5)	598.69(4)	671.94(10)	832.15(4)
Z′, Z	1,4	1,4	1,4	1, 4	1, 4
Density (g cm^{-3})	1.423	1.470	2.120	1.336	1.622
F(000)	232	232	368	280	408
Crystal size(mm^3)	0.3 × 0.3 × 0.3	0.3 × 0.3 × 0.	0.078 × 0.284 ×	0.3 × 0.3 × 0.3	0.3 × 0.3 × 0.3

		3	0.5		
θ (min, max)	2.54, 26.69	3.30, 30.12	2.37, 29.57	2.43, 30.11	3.03, 30.07
$h_{min, max}$, $k_{min, max}$, $l_{min, max}$	5, -5; 7, -7; 20, -18	-10, 10; -9,9; -12,12	4, -5; 11, -8; 23, -23	-12, 12; -5, 5; -5, 23	-18, 18; -10, 10; -10, 10
No. of ref.	7298	6554	6373	1643	13286
No. of unique ref./ obs. Ref.	966, 949	1306, 1127	1674, 1472	1643, 1513	2169, 1762
No. parameters	64	80	73	83	118
$\Delta\rho_{max, min}$ (eÅ^{-3})	0.185, -0.258	0.591, -0.260	0.474, -0.382	0.468, -0.505	0.246, -0.255
R_{int}	0.0268	0.0378	0.0233	-	0.0281
R_{all}, R_{obs}	0.0315, 0.0309	0.0449, 0.0375	0.0295, 0.0235	0.0940, 0.0893	0.0448, 0.0337
$wR2_{all}$, $wR2_{obs}$	0.0886, 0.0881	0.0983, 0.0940	0.0489, 0.0468	0.2285, 0.2264	0.0837, 0.0773
G.O. F	1.112	1.060	1.068	1.243	1.033

Table S4. Theoretical multipolar refinement parameters (Aspherical atom refinement).

Data	**Refinement**	**(1C)**	**(2A)**
Nobs, Nvar	Spherical atom refinement	1472,73	1513, 83
R(F2), wR(F2)		0.0295, 0.0489	0.0940/0.2150
G.O. F		1.067	1.238
$\Delta\rho_{max, min}$ (eÅ^{-3})		-0.382/0.474	-0.505/0.468
Nobs, Nvar	Multipolar Refinement	6290, 177	6672, 175
R(F2), wR(F2)		0.0026, 0.0022	0.0057, 0.0041
G.O. F		3.974	1.882
$\Delta\rho_{max, min}$ (eÅ^{-3})		-0.192/0.164	-0.181/0.141

S3. Differential Scanning Calorimetry (DSC)

DSC of four liquid compounds, namely, (**1A**), (**1B**), (**2A**), (**2B**) and one solid compound (**1C**) were recorded in a PerkinElmer 6000 DSC instrument, in hermetically open aluminium pan for (**1A**), (**1B**), (**2A**) and (**2B**), and a sealed aluminium pan for (1C) respectively and subsequently scanned at a rate of 3°C min^{-1} under a pure nitrogen purge (20 ml min^{-1}). DSC traces of (**1C**) and (**2A**) are shown in **Figure S4**. Because of the limitation in the intra cooler facility (minimum/lowest temperature reached is -25°C) of the instrument, the freezing point of the three liquid compounds, namely (**1A**), (**1B**) and (**2B**) could not be obtained. Among the four liquid compounds, we could obtain the freezing peak only for compound (**2A**), which has an onset freezing temperature of -19°C, as obtained from DSC. Compound (**1C**) is a low melting solid having an onset melting point of 45°C.

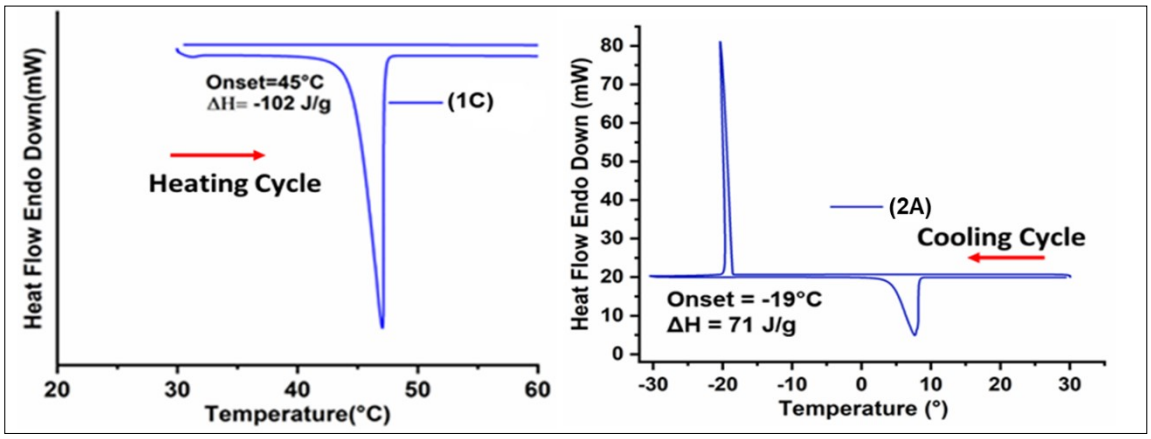

Figure S4. DSC trace of (**1C**) and (**2A**) at a scan rate of 3°C/min.

Table S5. Geometrical details and energetics of the associated interactions.

	Interactions	Symmetry element	Symmetry Code	D···A (Å)	H···A (Å)	D-H···A (°)	E_{tot}_CE (kJ/mol)
			(1A)				
1	C3-H3···O1#	translation	x+1, y-1, z	3.525(4)	2.48	162	-9.2
2	C4-H4···π(C3)	2_1‖ *a* axis	x+1/2, -y+1/2, -z+1	3.797(4)	2.86	169	-9.1
3	C5-H5···O1	2_1‖ *b* axis	-x, y-1/2, -z+3/2	3.460(4)	2.42	163	-7.1
4	S1···S1, O1···S1	2_1‖ *a* axis	x-1/2, -y+3/2, -z+1	3.687(1); 3.442(2)	-	100, 158 117, 152	-6.4
5	π···π (C4···C5)		x+1, y, z	3.484(4)	-	-	-5.1
			(1B)				
1	C3-H3···O1	-1	-x+1, -y+2, -z+1	3.390(2)	2.58	132	-18.8
2	π···π (C1···C2/S1···C5)	-1	-x+1, -y+1, -z+1	3.516(2) 3.548(1)	-	-	-15.0
3	C1-H1···O1, C5-H5···O1	2_1 ‖ *b* axis	-x+1/2, y-1/2, -z+ 3/2	3.381(2), 3.770(2)	2.38, 2.83	154, 146	-14.4
4	C4-H4···O1, C5-H5···S1	translation	x+1, y, z	3.330(2), 3.842(1)	2.51, 3.16	132, 125	-8.5
5	C1-H1···π(C4), S1···π (C3/C2)	2_1 ‖ *b* axis	-x+3/2, y-1/2, -z+3/2	3.599(2), 3.416(1)	2.87	127, 167	-7.5
6	C4-H4···π (C5), C5-H5···π(C3)	n-glide ⊥ *b* axis	x-1/2, -y+3/2, z+1/2	3.517(2), 3.687(2)	3.12, 3.09	112, 119	-4.2
			(1C)				
1	C5-H5···O1	-1	-x, -y+2, -z+1	3.481(2)	2.52	148	-19.8
2	π···π (C1···C5/C4···S1)	translation	x+1, y, z	3.509(2) 3.654(2)	-	-	-16.3
3	C4-H4···O1, S1···π (C4)	2_1‖ *b* axis	-x+1, y-1/2, -z+3/2	3.477(2), 3.547(2)	2.61	137; 154, 90	-10.2
4	C2-H2···Br1	-1	-x+2, -y+1, -	3.888(2)	3.24	127	-9.1

			z+1				
5	C4-H4···S1, S1···Br1	2_1 ‖ *b* axis	-x+2, y+1/2, -z+3/2	3.961(2), 3.625(6)	3.18	141; 166, 97	-7.5
6	O1···Br1		x-1, y+1, z	3.019(1)	-	173, 161	-6.1
(2A)							
1	C6-H6···π (C7)	-1	-x+1, -y+1, -z+1	3.589(7)	3.03	120	-16.4
2	π···π (C2···C7/C1···C4)	translation	x, y-1, z	3.450(7), 3.389(7)		-	-16.3
3	C3-H3···S1	-1	-x, -y+1, -z+1	3.742(5)	3.13	124	-12.8
4	C6-H6···S1	-1	-x+1, -y, -z+1	4.005(2)	3.09	161	-12.1
5	C3-H3···π (C3)	2_1 ‖ *b* axis	-x, y-1/2, -z+1/2	3.676(7)	2.88	142	-5.1
6	S1···π (C4)	*c*-glide ⊥ *b* axis	x, -y+1/2, z+1/2	3.527(5)	-	162, 95	-4.1
(2B)							
1	π···π (C5···C8), C4-H4···F2, F3···π(C5)	*c*-glide ⊥ *b* axis	x, -y+1/2, z-1/2	3.578(1) 3.340(2) 3.178(1)	- 2.70, -	- 117 -	-29.3
2	S1···π (C6)	-1	-x+1, -y+1, -z+1	3.638(1)	-	-	-16.0
3	S1···N1, (C8) π ···π (C8)	-1	-x+1, -y+1, -z+1	3.810(1) 3.775(1)	-	-	-16.0
4	C4-H4/C5-H5···F3, C5-H5···S1	translation	x, y-1, z	3.456(2), 3.363(2), 4.032(1)	2.85, 2.63, 3.28	116, 124, 138	-15.0
5	F2···F3, S1···F3	*c*-glide ⊥ *b* axis	x, -y+3/2, z+1/2	2.911(1), 3.482(1)	-	148,116;	-5.5
6	C6-H6···S1	2_1‖ *b* axis	-x+1, y-1/2, -z+3/2	3.914(1)	3.03	155	-4.1
7	C3 -H3···F1	2_1‖ *b* axis	-x+2, y-1/2, -z+1/2	3.370(1)	2.57	131	-4.1
8	S1···π (C8)	2_1‖ *b* axis	-x+1, y+1/2, -z+3/2	3.833(1)	-	-	-

* Geometric and energetic details are shown in blue shading in Table S4 as sulphur-centered interactions.

#: The hydrogen atoms positions are neutron normalized.

S4. Computational details and Topological analysis

Energy framework, Hirshfeld surface analysis, and 3D deformation density calculations were computed via Gaussian 09 suit [9] present in *Crystal Explorer* 21.5 [10] by using B3LYP/6-31G (d,p) level of theory for (1A) and (1B). In the case of (1C), together with the same density functional, the DGDZVP basis set was employed.

Further computational calculations such as AIMALL[11], NBO [12] were performed for all motifs *via* Gaussian 09 suit using the density functional M06-2X with 6-311G++ (d, p) basis set.

S5. d_{norm} plot, 3D deformation density and 2D finger print plot analysis

d_{norm} plot over the Hirshfeld surface reveals all the sulfur-centered contacts as shown in **Figure S5-S6** as weak van der Waals contact, indicative by blue-white surface. To understand the electronic nature of sulfur-centered interactions, a 3D deformation density plot has been mapped which reveals the charge-depleted (CD, red) and charge-concentrated (CC, blue) regions for all the molecules. It seems that for thiophenes discussed in this study, the aromatic regions do not fully incorporate the sulfur electrons into the π-system because there is a gap in the density between the sulfur atom and the two nearby carbon atoms in the 3D deformation density plot. Thus, the electronic structure seems to favour a scenario where sulphur interacts with a conjugated -C-C=C-C- butadiene system rather than integrating completely into the π-system, whereas in the -NCS containing molecules, the lone-pair of sulfur is fully delocalized into the -NCS moiety. In the case of (1A), the σ2 region is involved simultaneously in sulfur-centred interactions (S···S, S···O, **Figure S5**) involving the CC···CD interactions, with certain angularity, revealing chalcogen bonds. In case of (1B), σ1 region involves the formation of S···π interaction. In the case of (1C), the σ2 regions around the sulphur atom are involved in S···Br chalcogen bond (CC···CD) and σ1 region is involved in relatively weaker S···π contact. In maximum cases, the charge depleted (CD, red) region around the sulfur atom interacts with the charge-concentrated (CC, blue) region with a certain angularity (**Figure S5** (right side)). In case of (2A), very weak S···π contact is formed *via* σ3 region. In case of (2B), two types of S···π contact are mapped and, in both cases, sulfur acts as a Lewis base for S1···π(C6/C8) interaction (**Figure S6** (right side)).

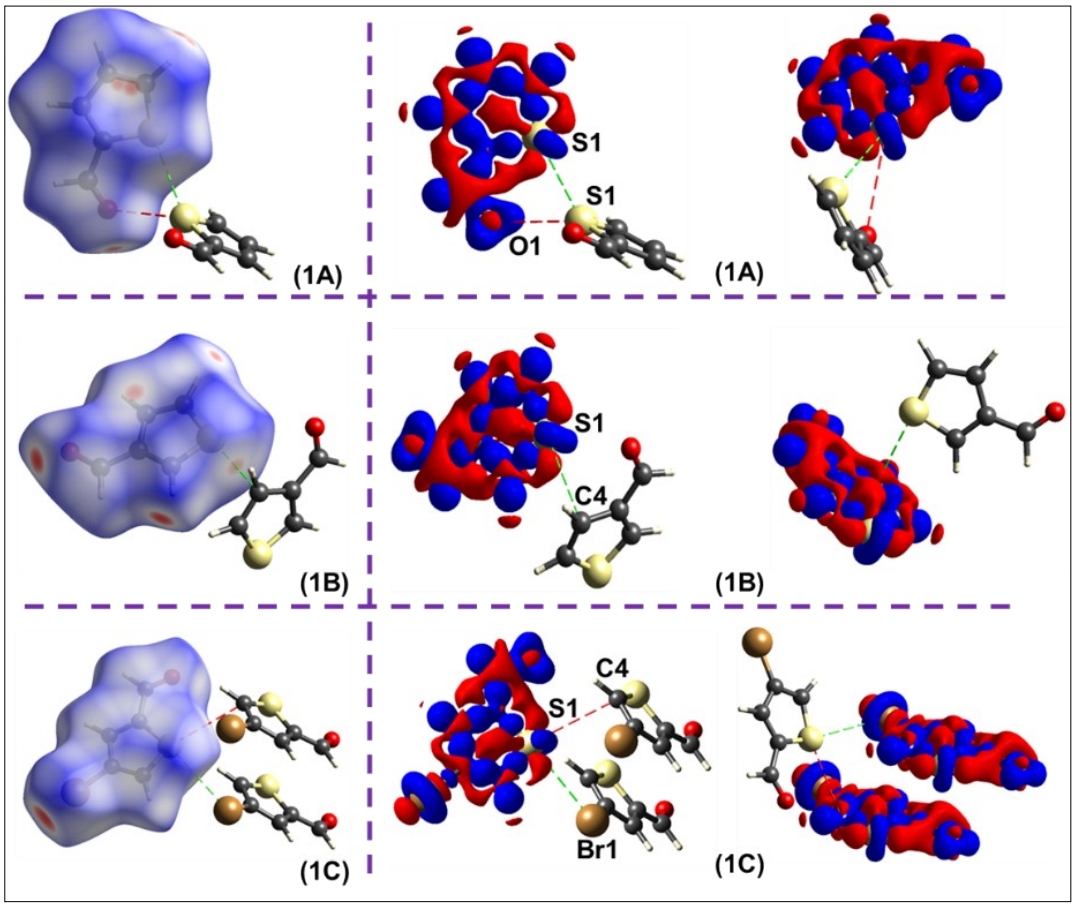

Figure S5. d_{norm} surface (left) showing pairwise sulfur centred interactions for (1A), (1B) and (1C). Red color on the surface indicates the involvement of shorter contacts (less than sum of the van der Waals radii) and 3D deformation density (right) for (1A), (1B) and (1C) over an isosurface of 0.008Å^3 showing charge concentrated region (blue) and charge depleted region (red) for sulfur centered interactions.

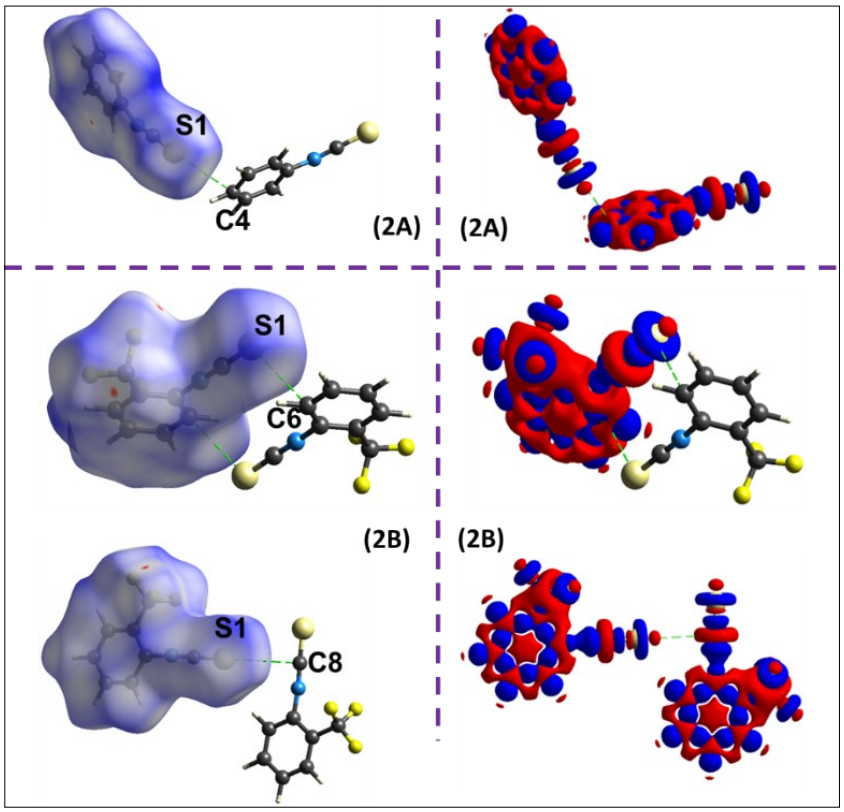

Figure S6. d_{norm} surface (left) showing pairwise sulfur centred interactions for (2A) and (2B). Red color on the surface indicates the involvement of shorter contacts (less than the sum of van der Waals radii) and 3D deformation density (right) for (2A) and (2B) over an isosurface of 0.008Å^3 showing charge concentrated region (blue) and charge depleted region (red) for sulfur centered interactions.

The 2D fingerprint plot extracted from the Hirshfeld surface depicts the greater contribution of C-H···O, C-H···π hydrogen bonding along with H···H contacts for (1A), (1B), (1C), (2A) and (2B) (**Figure S7**) and for the sulfur centered contacts it is shown in **Figure S8** along with the % contribution in **Figure S9**.

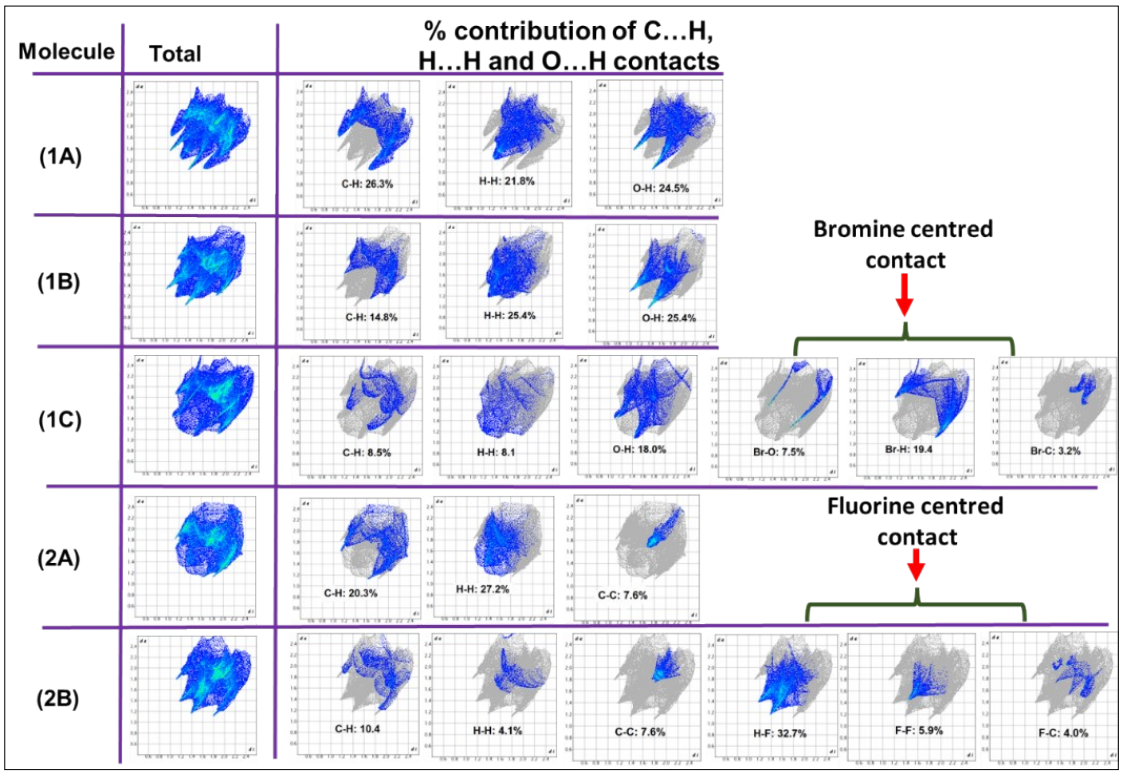

Figure S7. Fingerprint plot of (1A), (1B) and (1C) showing % of contributions of C···H, H···H, O···H, bromine centred and fluorine centered interactions.

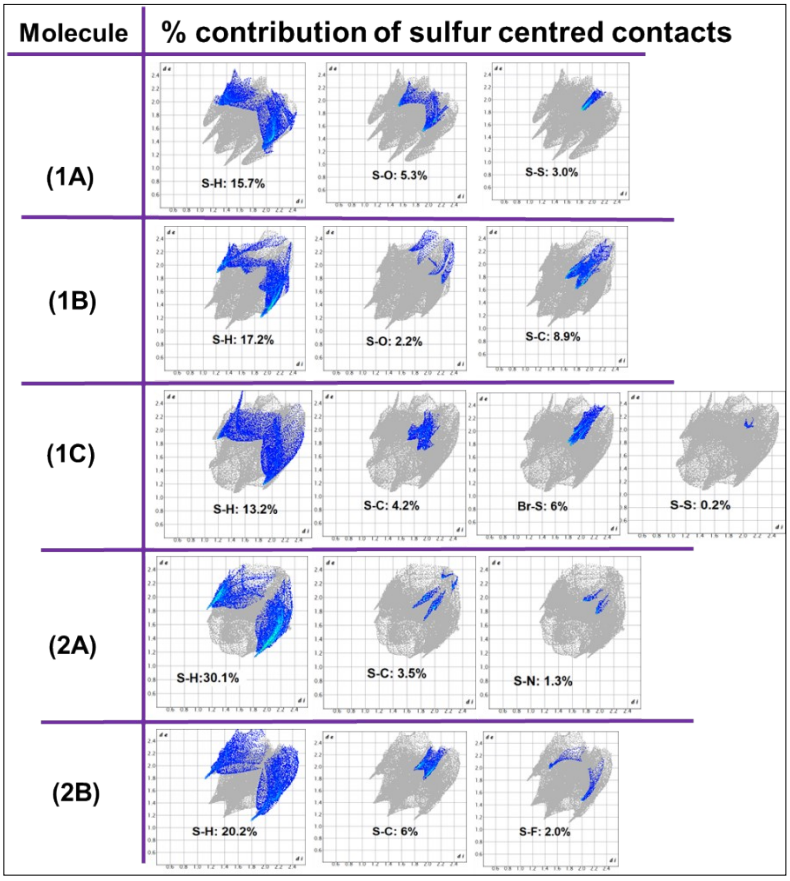

Figure S8. Fingerprint plot of (1A), (1B), (1C), (2A) and (2B) showing % contribution of sulfur-centered interactions.

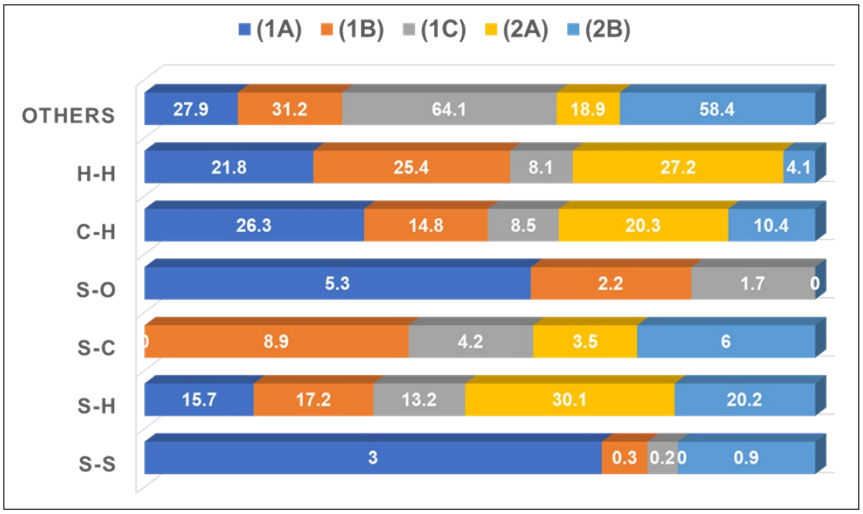

Figure S9. % contribution of sulfur centered and other interactions present in (1A), (1B), (1C), (2A) and (2B).

S6. Computation of Interaction Energies

To visualize the interaction energy topology at the crystal geometry, energy framework analysis has been performed using *Crystal Explorer* 21.5[10] (**Figure S10**). A 3.8 Å cluster is drawn by selecting kernel molecules using .cif file and the incomplete molecules are completed. The interaction energy is calculated by accurate energy model, which includes B3LYP/6-31G (d, p) for all systems except (1C) (B3LYP/DGDZVP). In this method, C-H bond lengths are normalized to neutron distances and the interaction energies are used to construct the three-dimensional topology of interactions that are termed as energy frameworks. The pairwise intermolecular interaction energies in the crystal structures are represented as cylinders joining the molecules. The radii of these cylinders are proportional to the strength of the intermolecular interaction. The tube size was set at the default value of 80, with an energy cut-off of 4 kJ mol^{-1}. The values are scaled factors for benchmarked energy models using k_ele=1.057, k_pol=0.740, k_disp=0.871, k_rep=0.618.

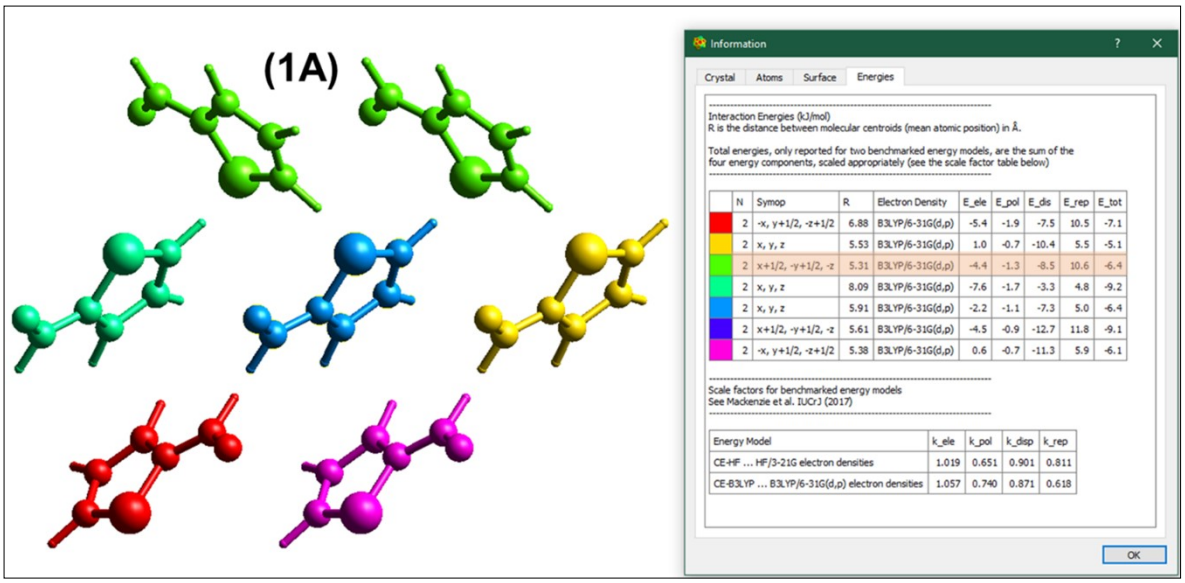

	N	Symop	R	Electron Density	E_ele	E_pol	E_dis	E_rep	E_tot
	2	-x, y+1/2, -z+1/2	6.88	B3LYP/6-31G(d,p)	-5.4	-1.9	-7.5	10.5	-7.1
	2	x, y, z	5.53	B3LYP/6-31G(d,p)	1.0	-0.7	-10.4	5.5	-5.1
	2	x+1/2, -y+1/2, -z	5.31	B3LYP/6-31G(d,p)	-4.4	-1.3	-8.5	10.6	-6.4
	2	x, y, z	8.09	B3LYP/6-31G(d,p)	-7.6	-1.7	-3.3	4.8	-9.2
	2	x, y, z	5.91	B3LYP/6-31G(d,p)	-2.2	-1.1	-7.3	5.0	-6.4
	2	x+1/2, -y+1/2, -z	5.61	B3LYP/6-31G(d,p)	-4.5	-0.9	-12.7	11.8	-9.1
	2	-x, y+1/2, -z+1/2	5.38	B3LYP/6-31G(d,p)	0.6	-0.7	-11.3	5.9	-6.1

Energy Model	k_ele	k_pol	k_disp	k_rep
CE-HF ... HF/3-21G electron densities	1.019	0.651	0.901	0.811
CE-B3LYP ... B3LYP/6-31G(d,p) electron densities	1.057	0.740	0.871	0.618

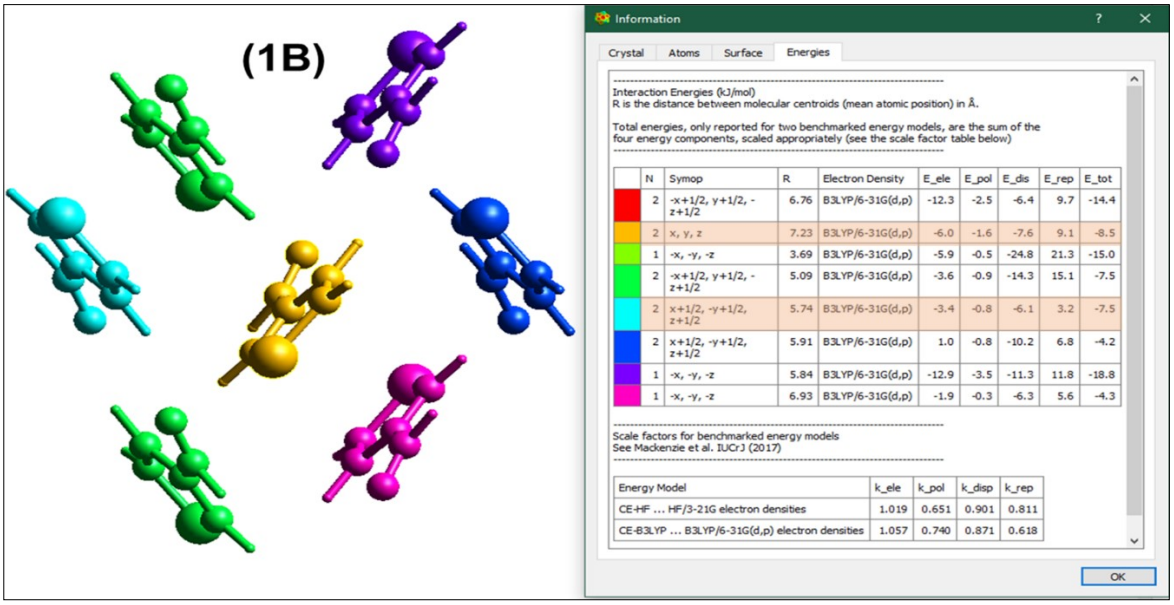

	N	Symop	R	Electron Density	E_ele	E_pol	E_dis	E_rep	E_tot
	2	-x+1/2, y+1/2, -z+1/2	6.76	B3LYP/6-31G(d,p)	-12.3	-2.5	-6.4	9.7	-14.4
	2	x, y, z	7.23	B3LYP/6-31G(d,p)	-6.0	-1.6	-7.6	9.1	-8.5
	1	-x, -y, -z	3.69	B3LYP/6-31G(d,p)	-5.9	-0.5	-24.8	21.3	-15.0
	2	-x+1/2, y+1/2, -z+1/2	5.09	B3LYP/6-31G(d,p)	-3.6	-0.9	-14.3	15.1	-7.5
	2	x+1/2, -y+1/2, z+1/2	5.74	B3LYP/6-31G(d,p)	-3.4	-0.8	-6.1	3.2	-7.5
	2	x+1/2, -y+1/2, z+1/2	5.91	B3LYP/6-31G(d,p)	1.0	-0.8	-10.2	6.8	-4.2
	1	-x, -y, -z	5.84	B3LYP/6-31G(d,p)	-12.9	-3.5	-11.3	11.8	-18.8
	1	-x, -y, -z	6.93	B3LYP/6-31G(d,p)	-1.9	-0.3	-6.3	5.6	-4.3

Energy Model	k_ele	k_pol	k_disp	k_rep
CE-HF ... HF/3-21G electron densities	1.019	0.651	0.901	0.811
CE-B3LYP ... B3LYP/6-31G(d,p) electron densities	1.057	0.740	0.871	0.618

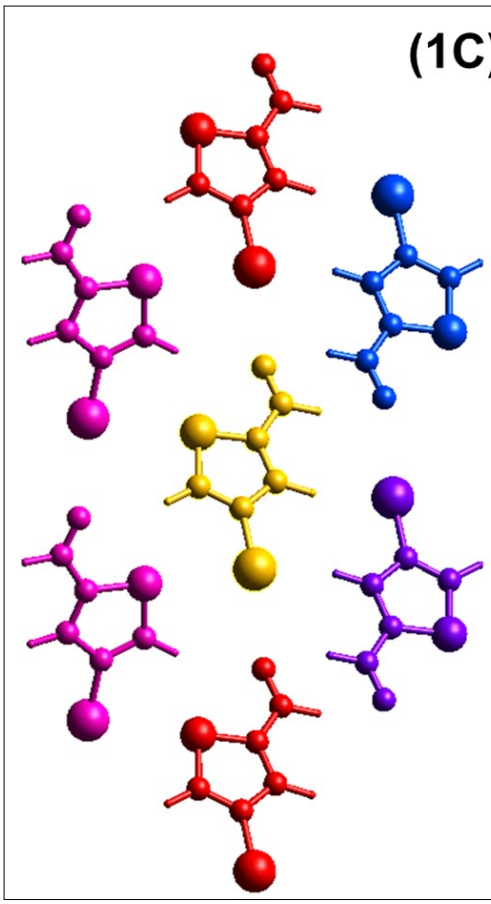

Information

Crystal | Atoms | Surface | Energies

Interaction Energies (kJ/mol)
R is the distance between molecular centroids (mean atomic position) in Å.

Total energies, only reported for two benchmarked energy models, are the sum of the four energy components, scaled appropriately (see the scale factor table below)

N	Symop	R	Electron Density	E_ele	E_pol	E_dis	E_rep	E_tot
2	x, y, z	9.44	B3LYP/DGDZVP	-9.2	-1.6	-3.6	12.8	-6.1
2	x, y, z	4.10	B3LYP/DGDZVP	-11.6	-0.8	-31.0	38.2	-16.3
1	-x, -y, -z	9.60	B3LYP/DGDZVP	-17.6	-2.6	-8.7	13.6	-19.8
1	-x, -y, -z	5.20	B3LYP/DGDZVP	-7.1	-2.0	-17.2	22.2	-10.2
2	-x, y+1/2, -z+1/2	6.18	B3LYP/DGDZVP	-13.6	-1.6	-12.6	18.7	-15.0
1	-x, -y, -z	7.89	B3LYP/DGDZVP	-7.6	-1.6	-11.4	10.0	-12.9
1	-x, -y, -z	5.55	B3LYP/DGDZVP	-5.7	-0.5	-11.6	12.2	-8.9
2	-x, y+1/2, -z+1/2	6.39	B3LYP/DGDZVP	-8.9	-0.8	-10.5	18.9	-7.5

Scale factors for benchmarked energy models
See Mackenzie et al. IUCrJ (2017)

Energy Model	k_ele	k_pol	k_disp	k_rep
CE-HF ... HF/3-21G electron densities	1.019	0.651	0.901	0.811
CE-B3LYP ... B3LYP/6-31G(d,p) electron densities	1.057	0.740	0.871	0.618

OK

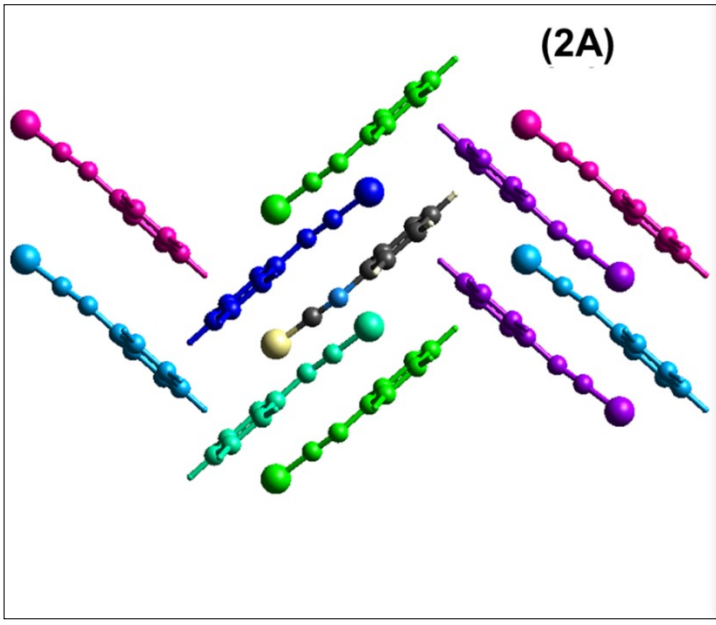

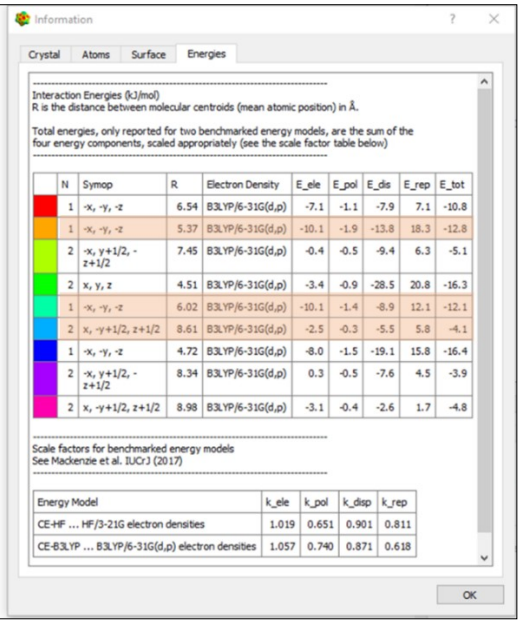

Information

Crystal | Atoms | Surface | Energies

Interaction Energies (kJ/mol)
R is the distance between molecular centroids (mean atomic position) in Å.

Total energies, only reported for two benchmarked energy models, are the sum of the four energy components, scaled appropriately (see the scale factor table below)

N	Symop	R	Electron Density	E_ele	E_pol	E_dis	E_rep	E_tot
1	-x, -y, -z	6.54	B3LYP/6-31G(d,p)	-7.1	-1.1	-7.9	7.1	-10.8
1	-x, -y, -z	5.37	B3LYP/6-31G(d,p)	-10.1	-1.9	-13.8	18.3	-12.8
2	-x, y+1/2, -z+1/2	7.45	B3LYP/6-31G(d,p)	-0.4	-0.5	-9.4	6.3	-5.1
2	x, y, z	4.51	B3LYP/6-31G(d,p)	-3.4	-0.9	-28.5	20.8	-16.3
1	-x, -y, -z	6.02	B3LYP/6-31G(d,p)	-10.1	-1.4	-8.9	12.1	-12.1
2	x, -y+1/2, z+1/2	8.61	B3LYP/6-31G(d,p)	-2.5	-0.3	-5.5	5.8	-4.1
1	-x, -y, -z	4.72	B3LYP/6-31G(d,p)	-8.0	-1.5	-19.1	15.8	-16.4
2	-x, y+1/2, -z+1/2	8.34	B3LYP/6-31G(d,p)	0.3	-0.5	-7.6	4.5	-3.9
2	x, -y+1/2, z+1/2	8.98	B3LYP/6-31G(d,p)	-3.1	-0.4	-2.6	1.7	-4.8

Scale factors for benchmarked energy models
See Mackenzie et al. IUCrJ (2017)

Energy Model	k_ele	k_pol	k_disp	k_rep
CE-HF ... HF/3-21G electron densities	1.019	0.651	0.901	0.811
CE-B3LYP ... B3LYP/6-31G(d,p) electron densities	1.057	0.740	0.871	0.618

OK

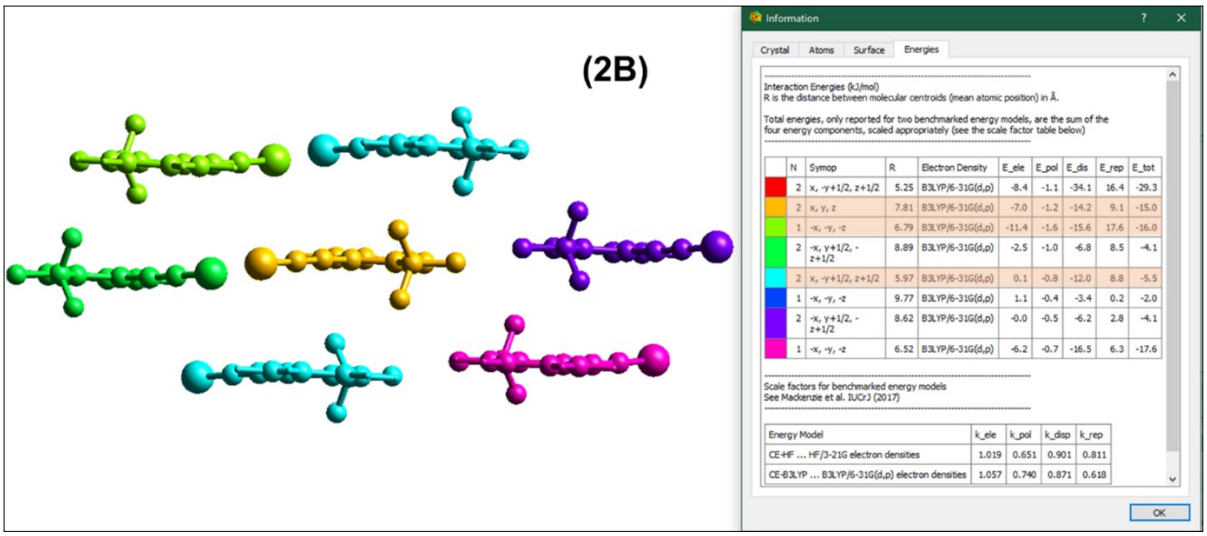

Figure S10. Interaction energy for (1A), (1B), (1C), (2A) and (2B) using B3LYP/631G (d, p) level of theory.

S7. Computation of Lattice energies

For lattice energy calculations, using *Crystal Explorer* 21.5, a 20Å cluster is drawn by selecting the kernel molecules using .cif files and the incomplete molecules are completed followed by summing up to obtain the lattice energy using B3LYP/631G (d, p) level of theory, as shown in **Table S2**.

S8. QTAIM

All the intramolecular bond critical points are shown in **Figure S11** for all the five molecules. This approach also helps to obtain the critical points for all the intermolecular interactions present in motifs A1, B1, C1, C2, C3, D1 and E1, using M062X/6311G++ (d, p) level of theory via AIMALL suit (**Figures S12** and **S13**). To compute the wavefunctions, .wfx and .fchk file have been used for all motifs, namely C1, C2, and C3 and A1, B1, D1 and E1 respectively, as input in AIMALL suit, by using M062X/6311G++ (d, p) level of theory. The topological analysis of the electron density $\rho(r)$ and its negative Laplacian $L(r) = -\nabla^2\rho(r)$ [13,14] were performed with AIMALL software. ρ_b and $\nabla^2\rho$ at bond critical points (r_b) signify the quantity of charge density and the local depletion ($\nabla^2\rho>0$) and concentration ($\nabla^2\rho<0$) of $\rho(r)$ at r_b. [15] The ratio $|V_b|/G_b$ is an important descriptor to classify interactions as closed-shell interactions ($|V_b|/G_b<1$), shared shell interactions ($|V_b|/G_b>2$) and intermediate interactions with partial degree of covalence ($1< |V_b|/G_b<2$) where V_b and G_b is the local potential and kinetic energy density. [16] The sulfur and halogen centred motifs have been analysed in the main manuscript and the rest are shown below. The ratio of $|V_b|/G_b$ clearly indicates that all interactions are

shown in **Table S6** are closed-shell interactions. **Table S7** and **S8** gives the quantitative estimates for the Laplacian distribution of ρ for the observed critical points corresponding to the σ-hole and the lone pairs on sulfur.

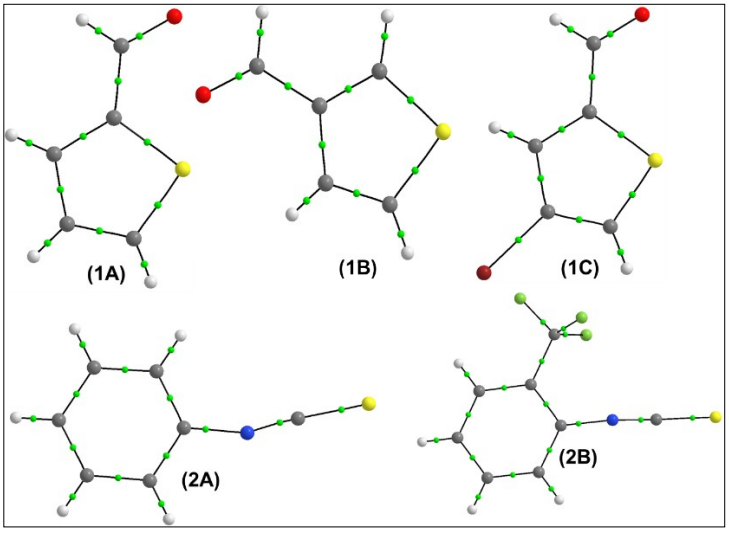

Figure S11. Molecular graph of (1A), (1B), (1C) (2A) and (2B) monomer. Green circles correspond to (3, -1) intra-molecular bond critical points.

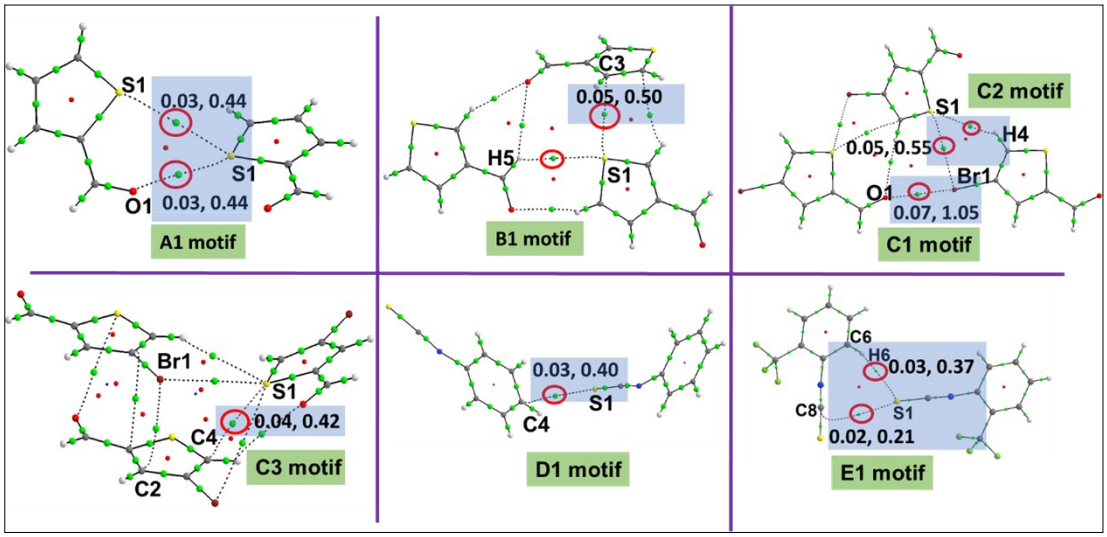

Figure S12. Molecular graph of motif A1, B1, C1, C2, C3, D1 and E1 illustrating sulfur centered and Br1···O1 contacts *via* the presence of bond critical (3, -1; green) and ring critical (3, +1; red) points. The BCPs are depicted in a red circle with a blue shaded area along with (ρ: e.Å^{-3}, $\nabla^2\rho$: e.Å^{-5}) values being mentioned for the observed chalcogen/halogen-bonded motifs.

Table S6. Topological parameters for different interactions present in A1, B1, C1, C2, C3, D1 and E1 motif.

Motif	Interaction	R_{ij} (Å)	ρ (e/Å^3)	$\nabla^2\rho$ (e/Å^5)	$\lvert V_b\rvert/G_b$
A1	S1···S1	3.508	0.04	0.44	0.73
	S1···O1	3.269	0.03	0.44	0.79
B1	H5···S1	3.024	0.03	0.31	0.74
	H1···(π)C4	2.782	0.04	0.39	0.81
	S1···C (π)	3.254	0.05	0.50	0.79
C1	Br···O	2.855	0.07	1.05	0.82
C2	H4···S1	3.032	0.03	0.31	0.72
	S1···Br1	3.439	0.05	0.55	0.79
C3	H4···O1	2.604	0.04	0.47	0.82
	Br1···π (C2)	3.536	0.04	0.38	0.76
	S1···C (π)	3.370	0.04	0.42	0.75
D1	S1···(π)C4	3.371	0.03	0.39	0.74
E1	H6···S1	2.886	0.03	0.37	0.76
	S1···(π)C8	3.994	0.02	0.21	0.65

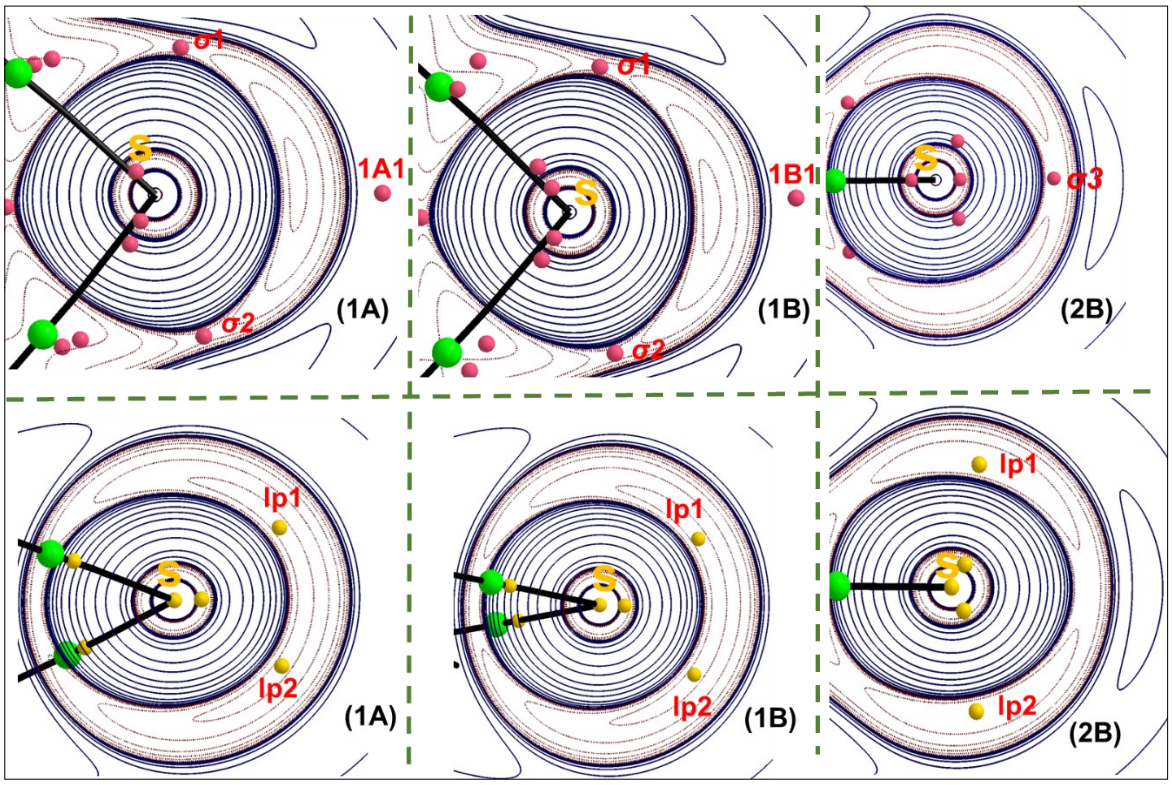

Figure S13. L(r) = - $\nabla^2\rho(r)$ maps [e/Å^5, contours are in logarithmic scale: positive (red) and negative (blue)] for (1A), (1B) and (2B) molecules (monomer). (3,+1) CPs in pink are mentioned as σ1 and σ2 for Set-1 molecules and σ3 for Set-2 molecules showing electrophilic regions (up) and (3, -3) CPs mentioned in yellow as lpn (where , n = 1-2) corresponding to the lone pairs of sulfur atom showing nuleophilic regions (in second row).

Table S7. Topological parameters for the *σ*-hole critical points on sulfur nuclei present in (1A), (1B), (1C), (T), (ThT), (2A) and (2B), signifying electrophilic power.

Molecules	Laplacian CPs	CPs type	ρ (e/ Å^3)	L (e/ Å^5)	L/ρ (Å^{-2})
(1A)	**σ1**	(3, +1)	0.87	1.31	1.5
	σ2	(3, +1)	0.88	1.28	1.5
	1A1	(3, +1)	0.35	1.69	4.83
(1B)	**σ1**	(3, +1)	0.87	1.36	1.6
	σ2	(3, +1)	0.87	1.24	1.4
	1B1	(3, +1)	0.35	1.66	4.74
(1C)	**σ1**	(3, +1)	0.86	1.31	1.5
	σ2	(3, +1)	0.88	1.28	1.5
	1C1	(3, +1)	0.35	1.71	4.89

(T)	**σ1**	(3, +1)	0.88	1.03	1.2
	σ2	(3, +1)	0.88	1.03	1.2
	T1	(3, +1)	0.35	1.64	4.69
(ThT)	**σ1**	(3, +1)	0.80	1.10	1.4
	σ2	(3, +1)	0.80	1.10	1.4
	ThT1	(3, +1)	0.35	1.66	4.74
(2A)	**σ3**	(3, +1)	0.94	3.99	4.2
	2A1	(3, +1)	0.34	1.47	4.32
	2A2	(3, +1)	0.34	1.47	4.32
(2B)	**σ3**	(3, +1)	0.95	4.22	4.4
	2B1	(3, +1)	0.34	1.49	4.38

Table S8. Topological parameters for the lone pair critical points for the sulfur nuclei present in (1A), (1B), (1C), (2A), (2B), (T), (ThT) signifying nucleophilic power.

Molecules	Lone pair	CPs type	ρ (e/ Å^3)	L (e/ Å^5)	L/ρ (Å^{-2})
(1A)	**lp1**	(3, -3)	1.23	11.3	9.2
	lp2	(3, -3)	1.23	11.3	9.2
(1B)	**lp1**	(3, -3)	1.23	11.3	9.2
	lp2	(3, -3)	1.23	11.3	9.2
(1C)	**lp1**	(3, -3)	1.23	11.3	9.2
	lp2	(3, -3)	1.23	11.3	9.2
(T)	**lp1**	(3, -3)	1.23	11.3	9.2
	lp2	(3, -3)	1.23	11.3	9.2
(ThT)	**lp1**	(3, -3)	1.34	13.8	10.3
	lp2	(3, -3)	1.34	13.8	10.3
(2A)	**lp1**	(3, -3)	1.16	9.5	8.2
	lp2	(3, -3)	1.16	9.5	8.2
(2B)	**lp1**	(3, -3)	1.16	9.5	8.2
	lp2	(3, -3)	1.16	9.5	8.2

S9. Theoretical Calculations

Theoretical Multipolar modelling of electron density in (1C) and (2A).

Theoretical structure factor calculations were performed at the TZVP [17,18] level using the CRYSTAL09 [19] package for both (**1C**) and (**2A**). Theoretical structure factors were subjected to the charge density modelling using the Hansen and Coppens multipole formalism in XD2016 [20]. All theoretical structure factors were assigned with unit weights and ADPs were set to zero to consider a static model during the multipolar refinements. The function $\Sigma\ w*\{|F_O|^2 - K|F_C|^2\}^2$, was minimized for all reflections. The core and valence scattering factors of all atoms in the multipole model were derived from Su, Coppens and Macchi wavefunctions [21]. The multipolar expansion was truncated at the hexadecapole level for Br and S atoms, at the octupole level for the C, N and O atoms, and at the quadrupole level for the H atoms for (1C) and (2A) molecules. Initially, chemically equivalent atoms were constrained in the multipole model. All multipoles, κ and κ′ were refined in a stepwise manner until convergence on the least square refinement was reached. The expansion/contraction of core electron densities of Br and S atoms were performed in stepwise to account the residual electron densities on Br and S sites in both compounds. The chemical constraints were released in the final stage, and the unconstrained refinement was found to be satisfactory. The correctness of the multipole model was verified by the residual density analysis and resulted in a flat and parabolic shaped fractal dimension plot [22], as shown in **Figure S14**. The residual electron density plots, deformation density plots and Laplacian plots are also shown in **Figure S14**. The topological parameters derived from the multipolar model for the two systems is compared with results from QTAIM and depicted in **Table S9**.

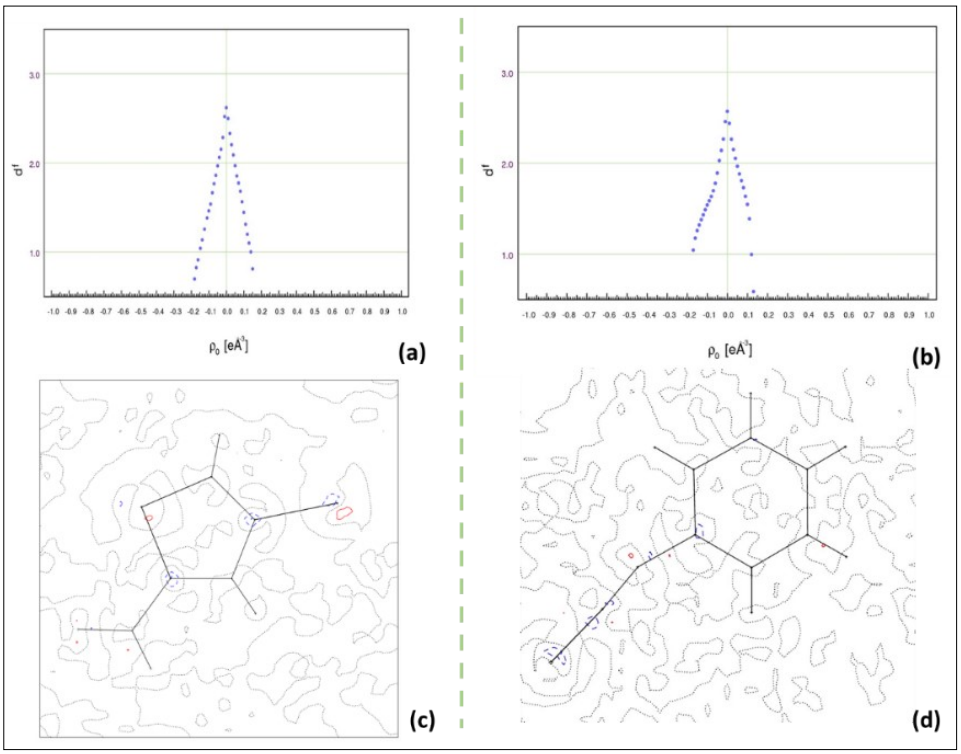
3.0
2.0
1.0
df
-1.0 -0.9 -0.8 -0.7 -0.6 -0.5 -0.4 -0.3 -0.2 -0.1 0.0 0.1 0.2 0.3 0.4 0.5 0.6 0.7 0.8 0.9 1.0
ρ0 [eÅ3]
(a)
(b)
(c)
(d)

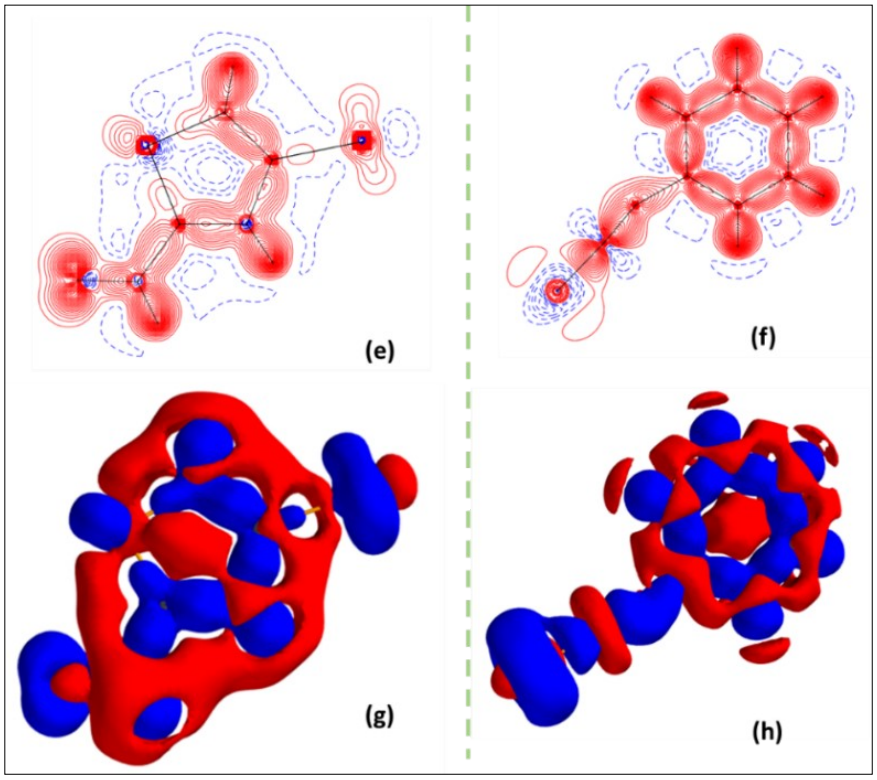
(e)
(f)
(g)
(h)

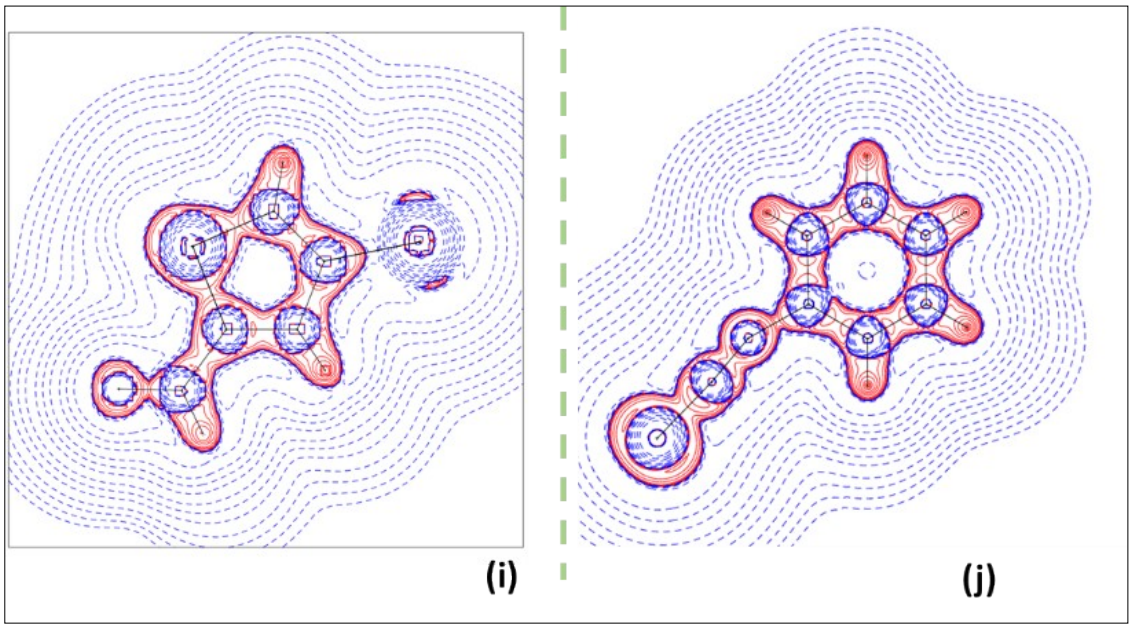

Figure S14. (a-b) Fractal dimensional plot, (c-d) Residual density plot, (e-f) 2D-static deformation density plot, (g-h) 3D-static deformation density plot (i-j) 2D-Laplacian map for (1C) and (2A) molecule respectively using theoretical multipolar model.

Table S9. Topological parameters obtained from QTAIM and Theoretical Multipolar model (in italics) for sulfur centered interactions in (C) and (D) molecules. R, ρ, $\nabla^2\rho$ and ε are bond path length, electron density at critical point, Laplacian and ellipticity respectively.

Molecule	Interactions	R(Å)	ρ (e/Å^3)	$\nabla^2\rho$ (e/Å^5)	ε
(1C)	C4-H4···O1	2.604	0.04	0.47	0.11
		2.709	*0.03*	*0.47*	*0.25*
	Br1···O1	2.855	0.70	1.05	0.08
		3.019	*0.84*	*1.07*	*0.01*
	S1···C4	3.370	0.04	0.43	0.43
		3.569	*0.03*	*0.38*	*0.13*
(2A)	S1···C4	3.371	0.03	0.34	0.37
		3.529	*0.04*	*0.40*	*0.21*
	C6-H6···S1	2.940	0.03	0.33	0.76
		3.093	*0.04*	*0.40*	*0.24*

S10. Natural Bonding Orbital (NBO) analysis:

Natural Bond Orbital analysis was performed via M06-2X/6-311G++(d, p) level of theory using NBO 6.0,[12] integrated with Gaussian 09 suit. Chemcraft visualization software [23] was used for plotting the bond orbitals between the interacting atoms.

For each donor NBO(i) and acceptor NBO(j), the stabilization energy associated with delocalization (i) →(j) is estimated as

$$E^{(2)} = \Delta Eij = q_i F\,(i, j)^{\,2} / (\mathcal{E}j - \mathcal{E}i)$$

Where q_i is the donor occupancy, Ɛi and Ɛj are diagonal elements (orbital energies) and F(i, j) is the off diagonal NBO Fock matrix elements.

The shifting of electron density from electron donor to acceptor atoms are supported via NBO 6.0 calculations shown in **Figure S15** and **Table S10**. S1···S1 and S1···O1 interactions represents the overlap between the nonbonding orbital *n*(S1/O1) and antibonding σ*(C1-S1) orbital respectively present in motif A1 [$E^{(2)}$; F(i,j): 0.17, 0.11 kJ/mol; 0.012, 0.008 respectively]. In case of B1 motif, sulfur centred interactions are the π(C3-C4)→σ*(S1-C4) and *n*(S1)→σ*(C5-H5) orbital interactions [$E^{(2)}$; F(i,j): 0.33, 0.29 kJ/mol; 0.013, 0.017 respectively]. Simultaneous formation of halogen bond and chalcogen bond via n(O1)→σ*(C3-Br1) and as n(Br1)→σ*(S1-C1) orbital interactions in motif C1 and C2 [$E^{(2)}$; F(i,j): 1.26, 0.86 kJ/mol; 0.032, 0.021 respectively]. Along with it, sulfur centred C-H···S and S···π interaction is revealed as n(S1)→σ*(C1-H1) in the same motif C2 [$E^{(2)}$; F(i,j): 0.29 kJ/mol; 0.018] and n(S1)→π*(C3-C4) orbital interaction in motif C3 [$E^{(2)}$; F(i,j): 0.07 kJ/mol; 0.007] respectively where sulfur atom act as a Lewis base. In case of D1 motif, π(C3-C4)→σ*(S1-C7) orbital interaction is observed with relatively significant amount of back donation. In case of D1 and E1, S···π interaction is revealed as π(C3-C4)→σ*(S1-C7) [$E^{(2)}$; F(i,j): 1.13 kJ/mol; 0.013] and n(S1)→σ*(C8-N1) [$E^{(2)}$; F(i,j): 0.34 kJ/mol; 0.008] respectively with significant magnitude of back donation.

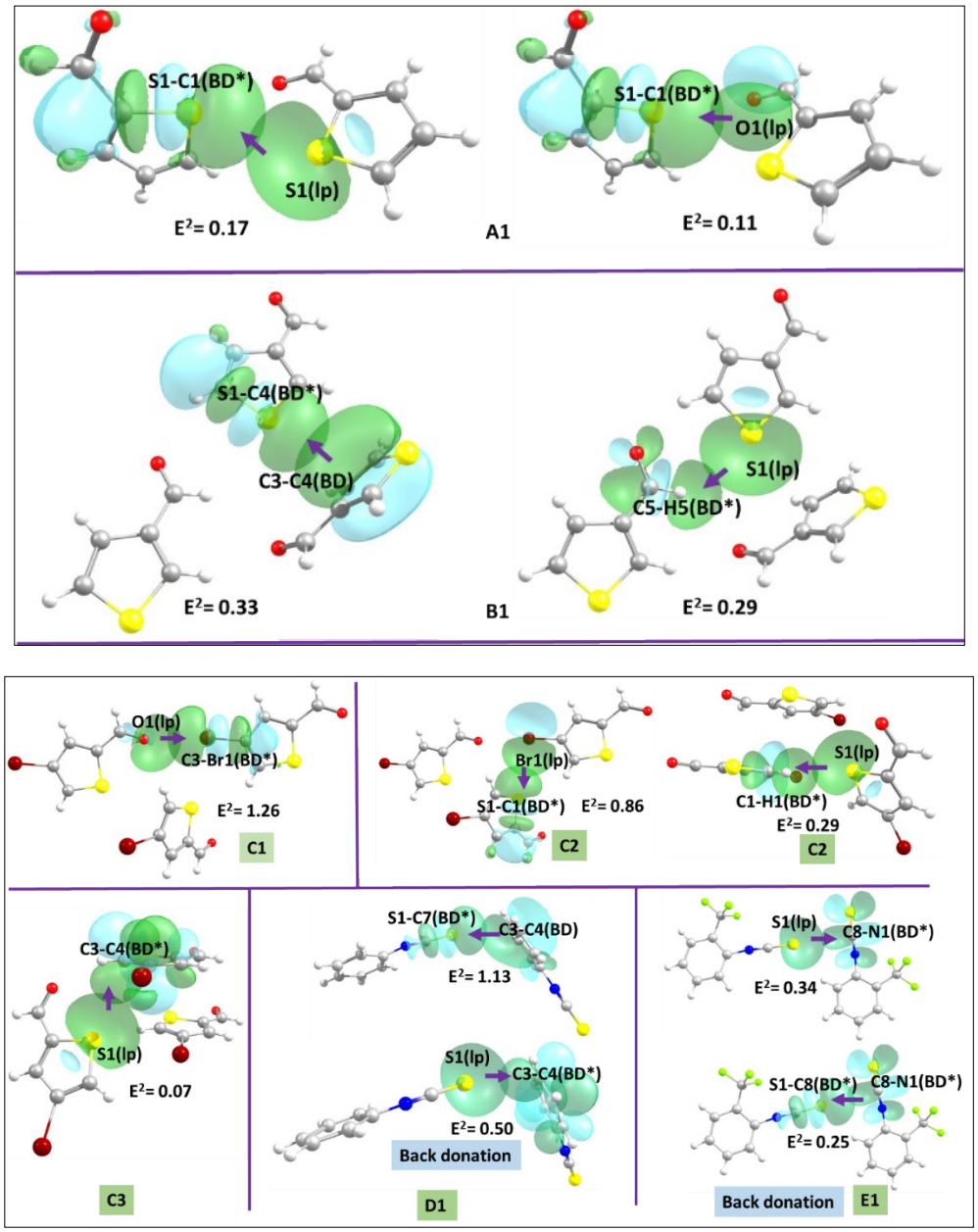

Figure S15. Orbital interactions present in sulfur and halogen centred motifs present in A1, B1 C1, C2, C3, D1 and E1. Violet arrow indicates donor to acceptor charge transfer.

Table S10. Second Order Perturbation Theory analysis of the Fock Matrix in NBO.

Motif	Donor NBO	Acceptor NBO	$E^{(2)}$ (kJ/mol)	E(j)-E(i)	F(i,j)
A1	S1(n)	S1-C1(σ*)	0.17	1.01	0.012
	O1(n)	S1-C1(σ*)	0.11	0.65	0.008
B1	C3-C4(π)	S1-C1(σ*)	0.33	0.64	0.013
	S1(n)	C5-H5(σ*)	0.29	1.28	0.017

C1	O1(n)	C3-Br1(σ*)	1.26	0.99	0.032
C2	Br1(n)	C3-S1(σ*)	0.86	0.62	0.021
	S1(n)	C1-H1(σ*)	0.29	1.48	0.018
C3	S1(n)	C3-C4(π*)	0.07	0.75	0.007
D1	C3-C4(π)	S1-C7(σ*)	1.13	0.69	0.013
E1	S1(n)	C3-C4(π*)	0.34	0.86	0.008

S11. Output of Atomic Laplacian of *ρ* CPs.

Monomer

(1A)

CP# = 10 (σ1)

Type = (3,-1)

Coords = 8.11603956884763E-01 -1.98738579755522E+00 -3.49652683294596E-02

DistFromNuc = 1.3690722293E+00

Rho = 1.2912695424E-01 (0.87 e/Å^3)

DelSqRho = -5.4362188453E-02 (-1.31 e/Å^5)

GradDelSqRho = -6.1964322562E-15 1.2212453271E-15 8.8297424927E-16

HessDelSqRho_EigVals = -7.2256769616E-01 -4.3974428392E-01 1.0238995425E+01

HessDelSqRho_EigVec1 = -1.3273619323E-01 9.9111566420E-01 8.4168398252E-03

HessDelSqRho_EigVec2 = 9.2312479761E-03 -7.2553983262E-03 9.9993106925E-01

HessDelSqRho_EigVec3 = 9.9110841338E-01 1.3280474156E-01 -8.1861805150E-03

</CP of DelSqRho>

<CP of DelSqRho>

CP# = 12 (σ2)

Type = (3,-1)

Coords = -1.64600589803252E+00 -2.98976331642992E+00 -2.14791916513591E-02

DistFromNuc = 1.3716053215E+00

Rho = 1.3026274929E-01(0.88 e/Å^3)

DelSqRho = -5.3261701327E-02 (-1.28 e/Å^5)

GradDelSqRho = -4.1633363423E-16 -9.4368957093E-16 -1.3877787808E-17

HessDelSqRho_EigVals = -7.5305259435E-01 -4.5980984235E-01 1.0098262377E+01

HessDelSqRho_EigVec1 = -5.9790287576E-01 8.0152878025E-01 7.9853362614E-03

HessDelSqRho_EigVec2 = 6.1507595418E-03 -5.3741215313E-03 9.9996664293E-01

HessDelSqRho_EigVec3 = 8.0154495777E-01 5.9793204735E-01 -1.7168080750E-03

</CP of DelSqRho>

<CP of DelSqRho>

CP# = 15 (lp1)

Type = (3,+3)

Coords = -1.45666070004155E-01 -3.16255560377348E+00 7.25501020579329E-01

DistFromNuc = 1.3047114652E+00

Rho = 1.8220068068E-01(1.23 e/Å^3)

DelSqRho = -4.6810875713E-01(-11.3 e/Å^5)

GradDelSqRho = 1.9678564334E-12 -4.8694659416E-12 4.6457768188E-12

HessDelSqRho_EigVals = 5.9510274997E-02 6.5738488448E-01 2.0002586515E+01

HessDelSqRho_EigVec1 = -2.2030120986E-01 5.2237851123E-01 8.2376457070E-01

HessDelSqRho_EigVec2 = 9.2519271664E-01 3.7943646570E-01 6.8121632852E-03

HessDelSqRho_EigVec3 = -3.0900778956E-01 7.6364170885E-01 -5.6689110638E-01

</CP of DelSqRho>

<CP of DelSqRho>

CP# = 16 (lp2)

Type = (3,+3)

Coords = -1.56744721204249E-01 -3.15216184605935E+00 -7.92591660382747E-01

DistFromNuc = 1.3048867350E+00

Rho = 1.8197810781E-01(1.23 e/Å^3)

DelSqRho = -4.6642200733E-01(-11.3 e/Å^5)

GradDelSqRho = 5.1320059313E-14 -1.2992384946E-13 -1.3622436512E-13

HessDelSqRho_EigVals = 5.2952330130E-02 6.5541363910E-01 1.9964829403E+01

HessDelSqRho_EigVec1 = 2.3243680353E-01 -5.3365392501E-01 8.1313382704E-01

HessDelSqRho_EigVec2 = 9.2500814263E-01 3.7964067119E-01 -1.5260958559E-02

HessDelSqRho_EigVec3 = -3.0055460143E-01 7.5570261949E-01 5.8187669008E-01

</CP of DelSqRho>

<CP of DelSqRho>

(1B)

CP# = 14 (σ1)

Type = (3,-1)

Coords = -3.48437637177712E+00 -2.07324101844528E+00 -7.57422925748072E-02

DistFromNuc = 1.3725756080E+00

Rho = 1.2940836729E-01(0.87 e/Å^3)

DelSqRho = -5.1274589570E-02 (-1.36 e/Å^5)

GradDelSqRho = -2.7755575616E-16 -3.3584246495E-15 6.9388939039E-16

HessDelSqRho_EigVals = -7.3504728806E-01 -4.6475926003E-01 9.9861219043E+00

HessDelSqRho_EigVec1 = 9.9366192604E-01 1.0756705242E-01 3.2639025434E-02

HessDelSqRho_EigVec2 = -3.1038430084E-02 -1.6521198310E-02 9.9938164175E-01

HessDelSqRho_EigVec3 = -1.0803977326E-01 9.9406055109E-01 1.3077773297E-02

</CP of DelSqRho>

<CP of DelSqRho>

CP# = 13 (σ2)

Type = (3,-1)

Coords = -4.44177728257956E+00 3.99494900366540E-01 -6.41089933113113E-02

DistFromNuc = 1.3706984939E+00

Rho = 1.2920820762E-01 (0.87 e/Å^3)

DelSqRho = -5.6366517292E-02 (-1.24 e/Å^3)

GradDelSqRho = -7.1321629158E-12 1.9170220966E-12 -3.3078401129E-13

HessDelSqRho_EigVals = -7.1926490629E-01 -4.3569956924E-01 1.0117347960E+01

HessDelSqRho_EigVec1 = 8.0758808175E-01 5.8899782751E-01 2.9716147215E-02

HessDelSqRho_EigVec2 = -2.7125892498E-02 -1.3236145247E-02 9.9954439142E-01

HessDelSqRho_EigVec3 = -5.8912280228E-01 8.0802621471E-01 -5.2877386005E-03

</CP of DelSqRho>

<CP of DelSqRho>

CP# = 17 (lp1)

Type = (3,+3)

Coords = -4.64649654058812E+00 -1.10722156721093E+00 6.67074374550752E-01

DistFromNuc = 1.3057715723E+00

Rho = 1.8253036659E-01 (1.23 e/Å^3)

DelSqRho = -4.7027987060E-01 (-11.3 e/Å^5)

GradDelSqRho = 1.2073675393E-15 2.6367796835E-16 -3.3306690739E-16

HessDelSqRho_EigVals = 5.9662421592E-02 6.7237719382E-01 1.9887209858E+01

HessDelSqRho_EigVec1 = 5.1879281345E-01 1.7708028951E-01 8.3635912608E-01

HessDelSqRho_EigVec2 = -3.5310120249E-01 9.3534966774E-01 2.0989041398E-02

HessDelSqRho_EigVec3 = 7.7857148516E-01 3.0620837697E-01 -5.4777994885E-01

</CP of DelSqRho>

<CP of DelSqRho>

CP# = 18 (lp2)

Type = (3,+3)

Coords = -4.60202010275295E+00 -1.08179940776168E+00 -8.52950039199562E-01

DistFromNuc = 1.3058459542E+00

Rho = 1.8236603462E-01 (1.23 e/Å^3)

DelSqRho = -4.6885065284E-01 (-11.3 e/Å^5)

GradDelSqRho = 1.2490009027E-15 2.1163626407E-16 6.5225602697E-16

HessDelSqRho_EigVals = 5.3915376918E-02 6.7040947972E-01 1.9865322246E+01

HessDelSqRho_EigVec1 = -5.6592471799E-01 -2.0662476401E-01 7.9814498712E-01

HessDelSqRho_EigVec2 = -3.5343105961E-01 9.3542252693E-01 -8.4369556577E-03

HessDelSqRho_EigVec3 = 7.4485951673E-01 2.8686391027E-01 6.0240633904E-01

</CP of DelSqRho>

<CP of DelSqRho>

(1C)

CP# = 8 (σ1)

Type = (3,-1)

Coords = 4.26866586380182E+00 1.82362529599620E+00 1.21647289159296E-02

DistFromNuc = 1.3703369038E+00

Rho = 1.2795627955E-01 (0.86 e/Å^3)

DelSqRho = -5.2110613196E-02 (-1.31e/Å^5)

GradDelSqRho = 3.3306690739E-12 -1.6850965068E-12 8.9234175604E-15

HessDelSqRho_EigVals = -6.9576524416E-01 -4.5617486150E-01 1.0096450522E+01

HessDelSqRho_EigVec1 = 5.0634249576E-01 8.6215451596E-01 -1.7517636602E-02

HessDelSqRho_EigVec2 = 5.4989605193E-03 1.7085634872E-02 9.9983890828E-01

HessDelSqRho_EigVec3 = 8.6231492995E-01 -5.0635725697E-01 3.9102293576E-03

</CP of DelSqRho>

<CP of DelSqRho>

CP# = 10 (σ2)

Type = (3,-1)

Coords = 2.38265382189792E+00 3.69601021024621E+00 -8.72178067254631E-03

DistFromNuc = 1.3715633398E+00

Rho = 1.3000817538E-01 (0.88 e/Å^3)

DelSqRho = -5.5988957000E-02 (-1.28 e/Å^5)

GradDelSqRho = 5.2269299999E-13 -2.0502488596E-12 2.6462859681E-13

HessDelSqRho_EigVals = -7.2703032442E-01 -4.5745625024E-01 1.0117773055E+01

HessDelSqRho_EigVec1 = 8.5928434624E-01 5.1137989961E-01 -1.1000481441E-02

HessDelSqRho_EigVec2 = 3.7393267158E-03 1.5225441029E-02 9.9987709414E-01

HessDelSqRho_EigVec3 = -5.1148453520E-01 8.5921986955E-01 -1.1170766620E-02

</CP of DelSqRho>

<CP of DelSqRho>

CP# = 12 (lp1)

Type = (3,+3)

Coords = 3.72483450426621E+00 3.18321073577706E+00 9.35448614593889E-01

DistFromNuc = 1.3067179881E+00

Rho = 1.8162777546E-01 (1.23 e/Å^3)

DelSqRho = -4.6712909996E-01 (-11.3 e/Å^5)

GradDelSqRho = 2.1094237468E-15 2.5535129566E-15 3.1086244690E-15

HessDelSqRho_EigVals = 9.9680498390E-02 6.2271283647E-01 1.9727652753E+01

HessDelSqRho_EigVec1 = 5.0199348220E-01 4.9335698605E-01 -7.1035303064E-01

HessDelSqRho_EigVec2 = 7.1079307150E-01 -7.0326439802E-01 1.3870688042E-02

HessDelSqRho_EigVec3 = 4.9272279563E-01 5.1187700749E-01 7.0370887153E-01

</CP of DelSqRho>

<CP of DelSqRho>

CP# = 14 (lp2)

Type = (3,+3)

Coords = 3.72462591989657E+00 3.16090374741278E+00 -9.37835270902735E-01

DistFromNuc = 1.3064603370E+00

Rho = 1.8192943552E-01 (1.23 e/Å^3)

DelSqRho = -4.6912785423E-01 (-11.3 e/Å^5)

GradDelSqRho = 5.5511151231E-16 5.5511151231E-16 -7.7715611724E-16

HessDelSqRho_EigVals = 1.0383473513E-01 6.2843026136E-01 1.9778381200E+01

HessDelSqRho_EigVec1 = -5.0119637586E-01 -5.1089646638E-01 -6.9841749224E-01

HessDelSqRho_EigVec2 = 7.1140330505E-01 -7.0277492959E-01 3.5687392534E-03

HessDelSqRho_EigVec3 = -4.9265356021E-01 -4.9506787310E-01 7.1568168248E-01

</CP of DelSqRho>

<CP of DelSqRho>

(2A)

CP# = 14 (σ3)

Type = (3,-1)

Coords = 8.19309907515716E+00 3.80285219207555E-01 -9.69991045000775E-02

DistFromNuc = 1.3437334324E+00

Rho = 1.3873302849E-01 (0.94 e/Å^3)

DelSqRho = -1.6562081300E-01 (-3.99 e/Å^5)

GradDelSqRho = -5.3290705182E-15 -6.5225602697E-16 1.0234868508E-16

HessDelSqRho_EigVals = -3.0080829690E-01 -2.7836099566E-01 1.2862526715E+01

HessDelSqRho_EigVec1 = -9.3233864268E-04 2.3088602093E-01 9.7298035750E-01

HessDelSqRho_EigVec2 = -1.3942310958E-01 9.6344755884E-01 -2.2875750890E-01

HessDelSqRho_EigVec3 = 9.9023246122E-01 1.3586922647E-01 -3.1292587607E-02

</CP of DelSqRho>

<CP of DelSqRho>

CP# = 19 (lp1)

Type = (3,+3)

Coords = 7.09559909105963E+00 7.49069425942596E-01 1.12411129046956E+00

DistFromNuc = 1.3223271886E+00

Rho = 1.7201530603E-01 (1.16 e/Å^3)

DelSqRho = -4.0006706871E-01 (-9.5 e/Å^5)

GradDelSqRho = -1.1102230246E-16 2.7755575616E-17 0.0000000000E+00

HessDelSqRho_EigVals = 1.3261201434E-02 4.4037596724E-01 1.7330900764E+01

HessDelSqRho_EigVec1 = 1.4505528684E-01 -9.0690652690E-01 3.9557491733E-01

HessDelSqRho_EigVec2 = 9.7134160191E-01 5.4442862474E-02 -2.3136868227E-01

HessDelSqRho_EigVec3 = 1.8829353724E-01 4.1779962444E-01 8.8881326365E-01

</CP of DelSqRho>

<CP of DelSqRho>

CP# = 20 (lp2)

Type = (3,+3)

Coords = 7.13422318512008E+00 -8.35941243873539E-02 -1.31825612906301E+00

DistFromNuc = 1.3224710633E+00

Rho = 1.7189516741E-01 (1.16 e/Å^3)

DelSqRho = -3.9916164169E-01 (-9.5 e/Å^5)

GradDelSqRho = 1.4507839374E-13 -1.3639089858E-13 -6.5818184236E-13

HessDelSqRho_EigVals = 1.2570992876E-02 4.3752509686E-01 1.7305557207E+01

HessDelSqRho_EigVec1 = 1.3493208834E-01 -9.6058583760E-01 2.4303946209E-01

HessDelSqRho_EigVec2 = 9.6671251586E-01 1.8143808939E-01 1.8040823538E-01

HessDelSqRho_EigVec3 = -2.1739421154E-01 2.1060642989E-01 9.5309217208E-01

</CP of DelSqRho>

<CP of DelSqRho>

(2B)

CP# = 15 (σ3)

Type = (3,-1)

Coords = -8.57348284760996E+00 -7.70214482430517E-01 1.29214387311254E-01

DistFromNuc = 1.3412942493E+00

Rho = 1.4030811454E-01 (0.95 e/Å^3)

DelSqRho = -1.7524382328E-01 (-4.22 e/Å^5)

GradDelSqRho = -6.4392935428E-15 7.9103390505E-16 2.6367796835E-16

HessDelSqRho_EigVals = -2.8085511846E-01 -2.6687968536E-01 1.3179143009E+01

HessDelSqRho_EigVec1 = 1.0446611322E-01 9.9205542193E-01 7.0091875544E-02

HessDelSqRho_EigVec2 = 3.2710715954E-02 -7.3866782885E-02 9.9673151222E-01

HessDelSqRho_EigVec3 = 9.9399036225E-01 -1.0183191157E-01 -4.0167418821E-02

</CP of DelSqRho>

<CP of DelSqRho>

CP# = 16 (lp1)

Type = (3,+3)

Coords = -7.37141153206285E+00 4.06792059437594E-01 1.45247500200309E-01

DistFromNuc = 1.3219855348E+00

Rho = 1.7136542429E-01 (1.16 e/Å^3)

DelSqRho = -3.9466153555E-01 (-9.5 e/Å^5)

GradDelSqRho = -2.2204460493E-16 1.7763568394E-15 1.8041124150E-16

HessDelSqRho_EigVals = 1.6339808069E-02 4.1575460121E-01 1.7328336137E+01

HessDelSqRho_EigVec1 = 3.3822161031E-02 -4.9735544719E-02 9.9818957970E-01

HessDelSqRho_EigVec2 = 9.9319330665E-01 1.1305729411E-01 -2.8019705289E-02

HessDelSqRho_EigVec3 = -1.1145903758E-01 9.9234289630E-01 5.3220852124E-02

</CP of DelSqRho>

<CP of DelSqRho>

CP# = 20 (lp2)

Type = (3,+3)

Coords = -7.63799662587453E+00 -2.16596470616891E+00 1.11735284382523E-02

DistFromNuc = 1.3220373453E+00

Rho = 1.7173573399E-01 (1.16 e/Å^3)

DelSqRho = -3.9750817046E-01 (-9.5 e/Å^5)

GradDelSqRho = -5.5511151231E-16 -7.7715611724E-16 -4.1633363423E-17

HessDelSqRho_EigVals = 1.9562339874E-02 4.2350633591E-01 1.7351939151E+01

HessDelSqRho_EigVec1 = 3.4255070255E-02 -6.1607352536E-02 9.9751246823E-01

HessDelSqRho_EigVec2 = 9.4905308368E-01 -3.1083150668E-01 -5.1788211089E-02

HessDelSqRho_EigVec3 = 3.1324883801E-01 9.4846629280E-01 4.7821092804E-02

</CP of DelSqRho>

<CP of DelSqRho>

Chalcogen and halogen bonding motif

(1A)

Motif A1

CP# = 11 (S1)

Type = (3,-1)

Coords = 1.78725774165600E+00 -5.78741727038528E-01 5.70866435717571E-01

DistFromNuc = 1.3713218084E+00

Rho = 1.2921287205E-01 (0.87 e/Å^3)

DelSqRho = -4.7892224817E-02 (-1.15 e/Å^5)

GradDelSqRho = -7.0499162064E-15 -5.4912671632E-15 3.8441472228E-15

HessDelSqRho_EigVals = -7.5214279349E-01 -4.6284347446E-01 1.0053528933E+01

HessDelSqRho_EigVec1 = -5.8033023070E-01 8.0711057452E-01 -1.0857874487E-01

HessDelSqRho_EigVec2 = 1.7231414041E-01 2.5200323660E-01 9.5226162674E-01

HessDelSqRho_EigVec3 = 7.9594262378E-01 5.3391655644E-01 -2.8532166129E-01

</CP of DelSqRho>

<CP of DelSqRho>

CP# = 16 (O1)

Type = (3,+3)

Coords = -1.96449137552999E+00 2.86427496511103E-01 3.83436974968793E+00

DistFromNuc = 6.4369070732E-01

Rho = 9.5677062277E-01 (6.46 e/Å^3)

DelSqRho = -5.3592426089E+00 (-129.14 e/Å^5)

GradDelSqRho = 1.8207657604E-14 -1.6875389974E-14 -2.2204460493E-14

HessDelSqRho_EigVals = 1.5269722880E+01 2.1218187098E+01 4.7473995196E+02

HessDelSqRho_EigVec1 = 7.7913926248E-01 -1.5726785044E-01 6.0680213652E-01

HessDelSqRho_EigVec2 = -5.2962054682E-01 -6.8298456916E-01 5.0302500403E-01

HessDelSqRho_EigVec3 = -3.3532683468E-01 7.1330141000E-01 6.1543237844E-01

</CP of DelSqRho>

<CP of DelSqRho>

CP# = 16 (S1)

Type = (3,+3)

Coords = -2.55542200388896E+00 -1.47406253634045E+00 -1.13945221621207E+00

DistFromNuc = 1.3051036433E+00

Rho = 1.8184910403E-01 (1.23 e/Å^3)

DelSqRho = -4.6492766120E-01 (-11.20 e/Å^5)

GradDelSqRho = 5.6191717945E-12 3.6584624219E-13 -1.5767387396E-12

HessDelSqRho_EigVals = 5.4758057316E-02 6.4979011357E-01 1.9920562545E+01

HessDelSqRho_EigVec1 = -1.1543346745E-01 8.8267186017E-01 -4.5559357091E-01

HessDelSqRho_EigVec2 = 2.1082436179E-01 4.6998088062E-01 8.5712954699E-01

HessDelSqRho_EigVec3 = 9.7068439931E-01 2.8912118402E-03 -2.4034025427E-01

</CP of DelSqRho>

<CP of DelSqRho>

(1B)

Motif B1

CP# = 15 (S1)

Type = (3,-1)

Coords = -7.18387526224697E-01 9.16769689143909E-01 -1.01627310859854E-01

DistFromNuc = 1.3728510023E+00

Rho = 1.2852235974E-01 (0.87 e/Å^3)

DelSqRho = -4.6479221134E-02 (-1.12 e/Å^5)

GradDelSqRho = -3.1918911958E-16 4.9960036108E-16 -1.6653345369E-16

HessDelSqRho_EigVals = -7.3372234940E-01 -4.7010531636E-01 9.9092076356E+00

HessDelSqRho_EigVec1 = 8.7941793958E-01 4.6376752867E-01 -1.0744192339E-01

HessDelSqRho_EigVec2 = -5.2129940504E-02 3.1815308513E-01 9.4660503048E-01

HessDelSqRho_EigVec3 = -4.7318765501E-01 8.2686050442E-01 -3.0396570427E-01

</CP of DelSqRho>

<CP of DelSqRho>

CP# = 15 (C3)

Type = (3,-1)

Coords = 3.12537147002684E+00 2.22438978983793E-02 1.90177715658934E+00

DistFromNuc = 1.0038829388E+00

Rho = 1.6694282457E-01 (1.12 e/Å^3)

DelSqRho = -8.5065578560E-02 (-2.04 e/Å^5)

GradDelSqRho = -2.2204460493E-16 6.6613381478E-16 4.4408920985E-16

HessDelSqRho_EigVals = -9.5107046321E-01 -2.1411116352E-01 1.4810651598E+01

HessDelSqRho_EigVec1 = -2.9479408285E-01 1.0619897574E-01 9.4964110393E-01

HessDelSqRho_EigVec2 = 6.4026584762E-01 7.5967695895E-01 1.1380053785E-01

HessDelSqRho_EigVec3 = 7.0933496536E-01 -6.4157049152E-01 2.9194384960E-01

</CP of DelSqRho>

<CP of DelSqRho>

(1C)

Motif C1

CP# = 14 (O1)

Type = (3,+3)

Coords = 9.46767540421721E-01 -1.62051024376658E+00 2.72259235738237E-01

DistFromNuc = 6.4173678310E-01

Rho = 9.6694479696E-01 (6.52 e/Å^3)

DelSqRho = -5.4540748923E+00 (-131.42 e/Å^5)

GradDelSqRho = 1.4210854715E-14 1.7763568394E-15 0.0000000000E+00

HessDelSqRho_EigVals = 1.5546539239E+01 2.1332399181E+01 4.8486106848E+02

HessDelSqRho_EigVec1 = 7.5478125618E-01 -6.5558292860E-01 -2.2721774665E-02

HessDelSqRho_EigVec2 = 4.3911911448E-02 1.5935311491E-02 9.9890830905E-01

HessDelSqRho_EigVec3 = 6.5450515609E-01 7.5495502487E-01 -4.0815573932E-02

</CP of DelSqRho>

<CP of DelSqRho>

Motif C2

CP# = 13 (S1)

Type = (3,-1)

Coords = -2.09326619641748E+00 4.27450264829958E-01 1.80281165146836E+00

DistFromNuc = 1.3720227582E+00

Rho = 1.2869869873E-01 (0.87 e/Å^3)

DelSqRho = -4.9207347018E-02 (-1.18 e/Å^5)

GradDelSqRho = -1.5019374633E-12 1.6601719999E-12 -6.4352689844E-13

HessDelSqRho_EigVals = -7.2206974936E-01 -4.6753136507E-01 1.0000185300E+01

HessDelSqRho_EigVec1 = 8.2035627450E-01 3.6086784362E-01 4.4361016932E-01

HessDelSqRho_EigVec2 = -4.5708000888E-01 -5.2387007844E-02 8.8788144867E-01

HessDelSqRho_EigVec3 = -3.4364727319E-01 9.3114445756E-01 -1.2196946658E-01

</CP of DelSqRho>

<CP of DelSqRho>

CP# = 21(Br1)

Type = (3,+3)

Coords = 1.19440900990350E+00 -2.05317108898048E+00 1.97097731292057E+00

DistFromNuc = 1.5595717148E+00

Rho = 1.6603806422E-01 (1.12 e/Å^3)

DelSqRho = -4.3032457071E-02 (-1.04 e/Å^5)

GradDelSqRho = 1.4988010832E-15 -1.0547118734E-15 5.2735593670E-16

HessDelSqRho_EigVals = 6.9814994477E-03 2.1770023001E-01 6.0307012636E+00

HessDelSqRho_EigVec1 = 1.5819553203E-01 5.4204612970E-01 8.2532427986E-01

HessDelSqRho_EigVec2 = 5.7509942985E-01 6.2886373425E-01 -5.2325046539E-01

HessDelSqRho_EigVec3 = 8.0264239822E-01 -5.5741940855E-01 2.1224698713E-01

</CP of DelSqRho>

<CP of DelSqRho>

Motif C3

CP# = 11(S1)

Type = (3,+1)

Coords = -4.64156057393493E-01 -5.77636547788455E-01 4.36743845433880E-01

DistFromNuc = 1.3018802018E+00

Rho = 1.8062800218E-01 (1.22 e/Å^3)

DelSqRho = -4.4997482254E-01 (-10.84 e/Å^5)

GradDelSqRho = -1.5543122345E-15 -2.2204460493E-16 -3.3306690739E-16

HessDelSqRho_EigVals = -6.1473168277E-02 6.6664338084E-01 2.0221668983E+01

HessDelSqRho_EigVec1 = -1.3805131971E-02 7.2384764032E-01 -6.8982172475E-01

HessDelSqRho_EigVec2 = -1.8726038540E-01 6.7580961163E-01 7.1289193914E-01

HessDelSqRho_EigVec3 = 9.8221329984E-01 1.3901784934E-01 1.2621834722E-01

</CP of DelSqRho>

<CP of DelSqRho>

CP# = 22 (C4)

Type = (3,-1)

Coords = 3.20344810590267E+00 -1.31823958090838E+00 -1.46181887946472E+00

DistFromNuc = 1.5945139323E+00

Rho = 7.6006987938E-02 (0.51 e/Å^3)

DelSqRho = 1.2533466933E-01 (3.02 e/Å^5)

GradDelSqRho = -6.1988608691E-13 -8.7493293860E-13 2.3598224069E-13

HessDelSqRho_EigVals = -1.1822759038E+00 -1.3604635402E-01 6.6103446153E-02

HessDelSqRho_EigVec1 = 8.5474419294E-01 3.2694650666E-01 -4.0313564271E-01

HessDelSqRho_EigVec2 = 3.8104922095E-01 1.3211984807E-01 9.1506602874E-01

HessDelSqRho_EigVec3 = -3.5243986133E-01 9.3576189681E-01 1.1654038744E-02

</CP of DelSqRho>

<CP of DelSqRho>

References

1 C. R. Groom, I. J. Bruno, M. P. Lightfoot and S. C. Ward, *Acta Cryst.*, 2016, **B72**, 171-179.

2 Apex2, Version 2 User Manual, M86-E01078, Bruker Analytical X-ray Systems Madison, WI, 2006.

3 G. M. Sheldrick, SADABS; Bruker AXS, Inc.: Madison, WI, 2007.

4 G. Sheldrick, *Acta Cryst.*, 2015, **C71**, 3–8.

5 O. V. Dolomanov, L. J. Bourhis, R. J. Gildea, J. A. K. Howard and H. Puschmann, *J. Appl. Crystallogr.*, 2009, **42**, 339–341.

6 C. F. Macrae, I. Sovago, S. J. Cottrell, P. T. A. Galek, P. McCabe, E. Pidcock, M. Platings, G. P. Shields, J. S. Stevens, M. Towler and P. A. Wood, *J. Appl. Crystallogr.*, 2020, **53**, 226–235.

7 M. Nardelli, *J. Appl. Crystallogr.*, 1995, **28**, 659.

8 A. Spek, *Acta Cryst.*, 2009, **D65**, 148–155.

9 M. J. Frisch, G. W. Trucks, H. B. Schlegel, G. E. Scuseria, M. A. Robb, J. R. Cheeseman, G. Scalmani, V. Barone, G. A. Petersson, H. Nakatsuji, X. Li, M. Caricato, A. Marenich, J. Bloino, B. G. Janesko, R. Gomperts, B. Mennucci, H. P. Hratchian, J. V. Ortiz, A. F. Izmaylov, J. L. Sonnenberg, D. Williams-Young, F. Ding, F. Lipparini, F. Egidi, J. Goings, B. Peng, A. Petrone, T. Henderson, D. Ranasinghe, V. G. Zakrzewski, J. Gao, N. Rega, G. Zheng, W. Liang, M. Hada, M. Ehara, K. Toyota, R. Fukuda, J. Hasegawa,

M. Ishida, T. Nakajima, Y. Honda, O. Kitao, H. Nakai, T. Vreven, K. Throssell, J. A. Jr. Montgomery, J. E. Peralta, F. Ogliaro, M. Bearpark, J. J. Heyd, E. Brothers, K. N. Kudin, V. N. Staroverov, T. Keith, R. Kobayashi, J. Normand, K. Raghavachari, A. Rendell, J. C. Burant, S. S. Iyengar, J. Tomasi, M. Cossi, J. M. Millam, M. Klene, C. Adamo, R. Cammi, J. W. Ochterski, R. L. Martin, K. Morokuma, O. Farkas, J. B. Foresman, and D. J. Fox, Gaussian, Inc., Wallingford CT, Gaussian 09, Revision A.02, 2016.

10 P. R. Spackman, M. J. Turner, J. J. McKinnon, S. K. Wolff, D. J. Grimwood, D. Jayatilaka and M. A. Spackman, *J. Appl. Crystallogr.*, 2021, **54**, 1006–1011.

11 T. A. Keith, AIMALL, version 13.05.06; TK Gristmill Software, Overland Park KS, aim.tkgristmill.com., 2013.

12 E. D. Glendening, C. R. Landis and F. Weinhold, *J. Comput. Chem.*, 2013, **34**, 1429–1437.

13 N. O. J. Malcolm and P. L. A. Popelier, *Faraday Discuss.*, 2003, **124**, 353–363.

14 P. L. A. Popelier, *Coord. Chem. Rev.*, 2000, **197**, 169–189.

15 E. Espinosa, E. Molins and C. Lecomte, *Chem. Phys. Lett.*, 1998, **285**, 170–173.

16 E. Espinosa, I. Alkorta, J. Elguero and E. Molins, *J. Chem. Phys.*, 2002, **117**, 5529–5542.

17 A. Schäfer, H. Horn and R. Ahlrichs, *J. Chem. Phys.*, 1992, **97**, 2571–2577.

18 M. F. Peintinger, D. V. Oliveira and T. Bredow, *J. Comput. Chem.*, 2013, **34**, 451–459.

19 R. Dovesi, V. R. Saunders, C. Roetti, R. Orlando, C. M. Zicovich-Wilson, F. Pascale, B. Civalleri, K. Doll, N. M. Harrison, I. J. Bush, M. Llunell, CRYSTAL 09 User's Manual (University of Torino, Torino, 2009).

20 A. Volkov and P. Coppens, *Acta Cryst.*, 2001, **A57**, 395–405.

21 P. Macchi and P. Coppens, *Acta Cryst.*, 2001, **A57**, 656–662.

22 K. Meindl and J. Henn, *Acta Cryst.*, 2008, **A64**, 404–418.

23 Chemcraft - graphical software for visualization of quantum chemistry computations. Version 1.8, build 648, https://www.chemcraftprog.com, 2014.